UNIVERSITAT POLITÈCNICA DE VALÈNCIA

Escuela Técnica Superior de Ingeniería del Diseño

Acoustic radiation minimization of railway wheels

by using advanced optimization techniques

Final Degree Project

Student: Jorge Gutiérrez Gil

Tutors: Enrique Nadal Soriano and José Martínez Casas

July 2017

Aknowledgements:

Abstract:

The environmentally-concerning rolling noise from the wheel-rail contact is a predominant source of train noise radiation, acting at a wide range of train speeds. The minimization of this effect due to changes on the wheel shape is discussed in this work, focused on potential shape modifications in already made wheels, in the form of an optimal perforation scheme on the web. Such post-manufacturing technique is a cost effective solution and can be performed in a relatively short term. A reduction of 1947% of the area below the acoustic power curves in the 0 to 5KHz range was achieved with the methods described in this project, which can be considered an important reduction.

Three main computational modules are connected together in order to develop an iterative optimization loop.
Firstly, the mesh generation tool creates a Finite Element (FE) discretization of a given wheel geometry. Candidate schemes of wheel perforations are defined through 4 variables: the perforation radius, its distance from the wheel's centre, the number of perforations radially arranged in one same row and the number of perforation rows.
Secondly, the acoustics solver module estimates the acoustic radiation in a range of frequencies of a given FE mesh, by calculating element surface speeds in their normal direction, after solving the wheel dynamics. This state of forced vibrations is excited by a wheel-rail contact force associated to a certain pseudo-random rail roughness.
Thirdly, a tuned Genetic Algorithm (GA)-based optimizer reads the result provided by the solver and proposes a new candidate design to the mesher module, in an acoustic power minimization strategy. In parallel, a structural analysis is performed for each candidate geometry, to check the von Misses stresses due to the Hertzian pressure imposed along the possible contact surface.

The work is structured as following: first we introduce the motivational aspects for the development of the project as well as the theoretical background supporting it. Then, the methodologies and models used for analysis are described and results are specified. Finally, a concluding discussion and future development are proposed.

Resumen:

El preocupante ruido de rodadura emitido por el contacto rueda-carril y frecuencias predominantes de radiación sonora en trenes, actuando en un amplio rango de velocidades. La minimización de este efecto debido a cambios en la geometría de la rueda es discutida en este trabajo, centrado en posibles modificaciones de ruedas ya fabricadas aplicando un patrón de perforación óptimo. Esta modificación *a posteriori* de la fabricación, se presenta como una solución económica y rápida en ejecución. Se ha alcanzado una reducción de hasta 1947% en el valor del área encerrada bajo la curva de potencia acústica en el rango de 0 a 5KHz, lo que puede considerarse una reducción importante.

Tres módulos de computación son conectados en serie de cara a desarrollar un lazo de optimiza iterativo.

Primero, un generador de mallas crea una discretización de elementos finitos (FE) a partir de una geometría de rueda conocida. Los esquemas de perforación candidatos se definen por medio de 4 variables, el radio de las perforaciones, sus distancias al centro de la rueda, el número de perforaciones radialmente organizadas en una misma fila, y el número de filas de perforaciones.

En segundo lugar, un módulo acústivo estima la radiación sonora del modelo propuesto, utilizando las velocidades normales de las superficies de la geometría, tras resolver previamente la dinámica de la rueda. Este estado de vibraciones forzadas es excitado por una fuerza de contacto rueda-carril asociada a una rugosidad pseudo-aleatoria del carril.

En tercer lugar, un optimizador basado en algoritmos genéticos (GA) interpreta el resultado obtenido por el módulo acústico y propone un nuevo candidato al generador de mallas, en una estrategia de minimización de la potencia acústica. En paralelo, se realiza un análisis estructural de fatiga para comprobar las tensiones de von Misses provocadas por una presión Hertziana impuesta en la posible superficie de contacto.

El presente trabajo se ha estructurado de la siguiente manera: primero se introducen los aspectos motivacionales del trabajo y el marco teórico en el que se basa. Después se describen las metodologías y modelos utilizados para el análisis y se especifican los resultados. Finalmente, se presentan las conclusiones y se proponen futuras mejoras.

Index:

Annex I: Articles and Conditions

Annex II: Budget

Annex III: Technical Drawings

1. Introduction and Scope

1.1   The acoustic environmental issue

Railway noise is a major cause for reduced comfort of residents around the railway network as well as passengers and operators. According to a recent report made by the European Parliament, around 12 million EU inhabitants are affected by railway noise during the day and 9 million during the night [1]. Also, in [2] it is estimated that 10% of the people in the EU live 'under serious annoyance' noise levels and that rail freight traffic is an important source of this noise.

Railway noise is also a barrier for railway infrastructure expansion, as government regulations often limit this type of hazardous environmental pollutant. Various national plan actions have been taken for noise abatement in countries within the EU [1] (pages 33-40), exemplifying the importance of noise reduction actions like the ones developed in this work. From all railway noise sources, rolling noise has been found to be the most important source [3].

1.2   Perforation as a sustainable and effective solution.

When re-designing railway wheels, a crucial factor to take in consideration is economy, due to the large-scale production nature of this industry. Manufacturing a totally new wheel design which minimizes noise as much as the most sophisticated optimization tools permit, will probably suppose an important investment. Moreover, these solutions may even require new manufacturing processes or train designs, delivering an environmental and economic profit only in the long-term.

The present work focuses mainly on an optimized shape modification, precisely an optimized scheme of perforations in its web. This modification can be performed in already manufactured wheels, enabling a quick and effective noise minimizing solution with very little cost. It can be very promising particularly in geographical areas whose inhabitants are actually affected by train noise and cannot wait for the time needed to manufacture and implement a completely new wheel design. The optimized scheme of perforations presented here is designed to suit a specific wheel model. However, the methodologies explained in this work can be extrapolated to other similar wheel designs.

It is assumed that web perforation is an effective measure to reduce noise mainly because it interrupts the continuity of the wheel disc, reducing its radiation surface. Due to a specifically designed set of holes in the web, the vibrating wheel web will displace air in a different manner, potentially resulting in a less

unpleasant sound radiation for humans. This effect is often marked in literature as 'acoustic short-circuiting' [3] (Ch. 7.4 page 254). A perforation study in the wheel for acoustic radiation reduction has been studied before [4-6] with some promising results, but a full-scale optimization study has not been achieved yet with successful results according to the author's knowledge.

Although this technique can minimize sound radiation, a careful attention must be paid to structural stresses. Due to the fact that the wheel is being perforated, material is being subtracted thus the reduced stiffness can potentially bring an undesired deformations or fracture scenario. Mechanical resistance to fatigue is studied in parallel with noise reduction in a procedure later developed.

1.3   Developing a shape optimization study

Shape optimization using computational techniques has been widely explored in research and industry [7-9] as a potent tool to provide highly effective outcomes even when there are many design variables, when the objective functions require advanced mathematical solving tools and when there are a high number of constraints to the solution.

Algorithms, which are usually employed in shape optimization, include Genetic Algorithms (GA), Gradient-Based Methods (GM) and Simulated Annealing (SA), among others [8]. The effectiveness and efficiency of these algorithms rely on the type of design problem. These, along with other techniques linked with Artificial Intelligence (AI) are of a great interest for present and future applications of major importance.

The problem approached in this work is the shape optimization of a railway wheel with regards to dynamic mechanics and acoustics, ultimately to minimize the sound power emission. A similar problem has been treated before with the use of GA [10] and Response Surface Models (RSM) [11], along with other examples in literature. In the present work, GA are used in order to avoid the calculation of derivatives with respect to the parameters optimized, which involves complex calculi.

As GA requires of tuning different parameters for a better performance, the optimization study in this work extends the specific knowledge for this type of applications through testing various tunings. Moreover, an optimization study through a GA-driven sound power minimization of railway wheels through a perforation scheme optimization has not been researched before, to the extent of the author's knowledge.

2. Theoretical Background

This chapter summarizes the theory on which the work is based, mainly related to applied acoustics, railway dynamics and structural resistance.

2.1   The acoustic phenomena.

2.1.1   Noise impact on humans.

Introduction

Noise is sound which can be harmful and which is unwelcome. There is not a fixed value at which sound is perceived as noise, but there are a series of parameters which affect the annoyingness of sound, such as sound pressure level, duration, frequency and bandwidth. The annoyingness also depends on the individual perception, as psychology also affects our perception and tolerance to sound. Some sound power values are usually taken to measure how harmful a noise is, and those are summarized in Table 1 and follow the long-term A-weighted average measurements defined by ISO 1996-2:1987.

Long-term exposure to noise between 55 and 75 A-weighted decibels (dB(A)) can derive in physiological effects such as discomfort, arterial hypertension and stomach ulcers [1]. Usually, railway noise power can reach levels of 100 dB(A) depending on many factors from which the wheel design is a major one, as it will be seen later.

Noise power level.		Effect.
0 dB(A)	- - - - - -	Faintiest audible sound
45 dB(A)	- - - - - -	Bound for health hazards
55 dB(A)	- - - - - -	Bound for noise pollution
65 dB(A)	- - - - -	
75 dB(A)	- - - - -	Stress to the human body
90 dB(A)	- - - - -	Bound for hearing protection utilization in workplace
120 dB(A)	- - - -	Bound for risk of injury
150 dB(A)	- - - -	Possible eardrum rupture

Table 1. Typical effects of noise power levels on humans. Edited from the information on [1].

A-weighted sound pressure level

When quantifying the intensity of noise which can potentially be a human hazard, it is required to account how human beings react to sound along the frequency domain. The human hearing system is less sensible to low and very high frequencies and highly sensible to medium-high frequencies. The A-weighted sound pressure level, dB(A) has become the predominant standard used in noise analysis in engineering, as this type of weighting is one effective way to relate the measured sound power level and human annoyance. It is based in the frequency-dependent, non-linear sensibility of the human hearing system. The dB(A) weighting function, or dB(A) filter is shown in Figure 1.
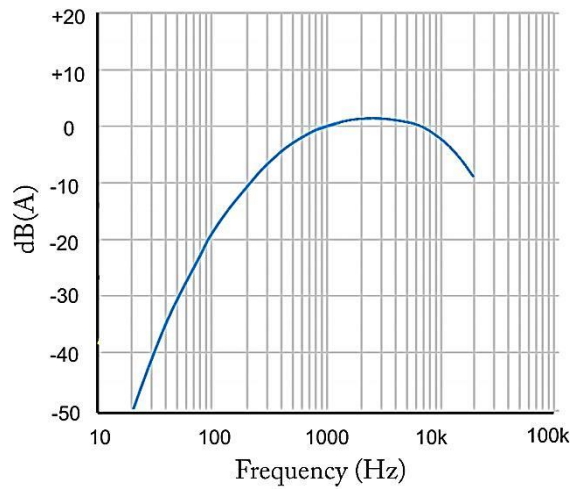
Figure 1. The dB(A) weighting function for a range of different frequencies. Edited from the data in [13].

For industrial equipment for noise evaluation, the revised dB(A) weighting functions in [13] are used. They are based on the actual standard IEC 61672-1:2013 and correspond to equations (X and X). Equation 1 is a weighting function applied to the amplitude spectrum of the unweighted sound level. Equation 2 is then used to normalise the response of the filter to 1 KHz accounting for the loss of 2 dB at 1 KHz.

$$R_A(f) = \frac{12194^2 f^4}{(f^2 + 20.6^2)\sqrt{(f^2 + 107.7^2)(f^2 + 737.9^2)}(f^2 + 12194^2)} \tag{1}$$

$$A(f)[dB] = 20\log_{10}(R_A(f)) + 2 \tag{2}$$

Where $R_A(f)$ is the weighting function applied to the amplitude spectrum, f is the frequency in Hertz and $A(f)$ is the A-weighted intensity in dB(A). In this work a hearing threshold of 10^{-12} Wm^{-2} at 1 KHz was set as a reference for the dB(A) scale.

2.1.2 Sources of railway noise

Rolling noise.

Rolling noise is considered the most important source of noise in railway traffic [3], thus the object of improvement in this work. It is caused by the vibrational displacement of air by the wheel and rail, an effect comparable to a percussion instrument. This air is displaced by high frequency vibrations of rail and wheel. These forced vibrations, due to the contact forces (or interaction forces) between both elements, are caused by the roughness of the surface of both the wheel and the rail [3], between other factors.

A simplified and adapted version of the wheel rolling noise generation model in [3] is shown in Figures 2 and 3. The effect of rail noise is not the main focus of this work, so the Figures have been adapted to this fact, acknowledging however the existence of noise production by the rail. The mathematical description of the noise production mechanism by the wheel is discussed later.
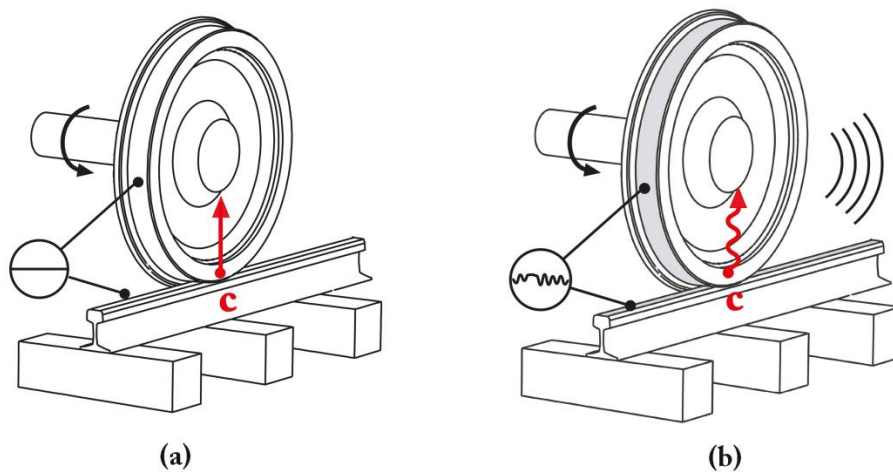
Figure 2. Illustrative representation of the rolling noise generation mechanism explained in [3] (Chapter 2). (a) is representing a (theoretical) constant contact force due the smooth wheel and rail surfaces, where (b) shows a contact caused by (real) rough surfaces , causing a dynamic force of certain frequency content.
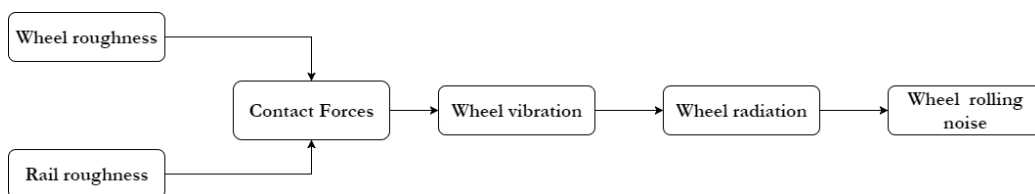
Figure 3. Block diagram of a simplified version of the rolling noise generation model explained in [3] (Chapter 2).

Roughness

Typical wavelengths of roughness relevant to rolling noise are between about 5 and 500 mm and its amplitudes are of the order of 10^{-4} times the wavelength, therefore not apparent to the human eye. The effect of manufacturing tolerances and irregular wear of both wheel and rail surfaces are the main sources of roughness. There are two main types of roughness present at this range of wavelengths:

- Corrugation, also called quasi-periodic roughness or macro-roughness is the *undesired* type of roughness with peak-to-trough amplitudes of typically 50 μm at a wavelength of 50 mm.
- Short wavelength corrugation, or micro-roughness, of less than 1 mm of wavelength, is typically not related with rolling noise and is a *desired* type of corrugation due to its importance for electric conductivity and traction.

Some authors target noise reduction through roughness reduction by techniques like re-profiling [14], but this discussion is not the aim of this work. As a totally rough surface is not possible to achieve in practical terms, rolling noise is a constant problematic to be solved in railway traffic.

Wheel and rail rolling noise radiation.

Although it is true that both wheel and rail contribute significantly to the overall rolling noise production, the wheel has a significantly more important effect on the high frequency band (above 1KHz) while the rail has an effect in the whole frequency spectrum [3]. In [15] this pattern is demonstrated, giving in this case a higher importance to the rail noise radiation. In [16] the relationship with speed of the noise produced by the two elements (wheel and rail) is analysed, where a clear predominance of the wheels is seen at high speeds, which are related with high frequencies. In the present work, only the wheel acoustic radiation is a target to minimize, however, the rail is also an important element to be optimized in order to further reduce the total rolling noise emission.

Speed dependence on rolling noise

As the speed of the train increases, so does the frequency of the interaction forces and thus the A-weighted sound pressure level which is usually taken to be proportional to the logarithm of the speed, as shown in Equation 3 (from [3]):

$$A = A_0 + N \, log_{10} \left(\frac{V}{V_0} \right) \tag{3}$$

Where A_0 is the sound level at a reference speed V_0 . N accounts for the speed 'exponent' and typically is 30.

Also, from the comprehensive work done by Thompson in [3] it has been noticed that there is a clear difference in the type of wheel depending on the type of braking system it uses. In general, vehicles with tread braking produce the highest amount of rolling noise, followed by disc-braked vehicles and drum braked trains, which are the least noisy.

Wheel design dependence in rolling noise.

Noise reduction through wheel shape design modification is the main objective of this work, it is therefore relevant to describe the state of the art on knowledge of the relationship of wheel characteristics (not only shape, but material modifications or added parts) affecting noise radiation. Wheel shape optimization has shown in literature levels of noise reduction, which depends on the technique used. Different physical effects which reduce noise can be targeted when proceeding with wheel shape optimization to reduce rolling noise, mainly: decoupling radial and axial motions of wheel and axis respectively, to 'alienate' the wheel's natural frequencies by increasing them, reducing the radiating area, shielding the radiated noise, and acoustic short-circuiting by means of shape modifications. The following are some results obtained with these methods:

- Increasing natural frequencies through axle diameter reduction produced a noise reduction of 10dB in [17].
- Slightly reducing wheel diameter produced reductions of 3dB of total rolling noise due to wheel noise contribution [19].
- Shielding the radiated noise with cover plates along with shape optimization was researched by [6] and yielded a noise reduction of 8dB.

Wheel shape optimization though perforation is studied, (but not extensively explored) in the work reviewed in [6] (Silent Freight EU project) (Figure 4, (a)), concluding that perforations produced a decrease in noise production only in lower frequencies due to the decreased radiation efficiency, but didn't have a relevant effect in the higher frequency domain, where the wheel noise contribution is dominant. In [5] perforation was more extensively explored with more promising results, but an optimization study was not carried out to explore how the number, positioning or diameter of holes influenced noise production.

Wheel damping has also been researched previously, and proved to reduce noise levels. These include systems based on constrained layer damping applied on the wheel web achieving reductions in the range of 1-8dB [19], tuned absorbers mounted on the inside of the tyre or on the web, achieving 4-5dB of reduction [20] or laminated cover plates and various 'friction' dampers. These kinds of techniques are not covered in this work but are worth to mention.
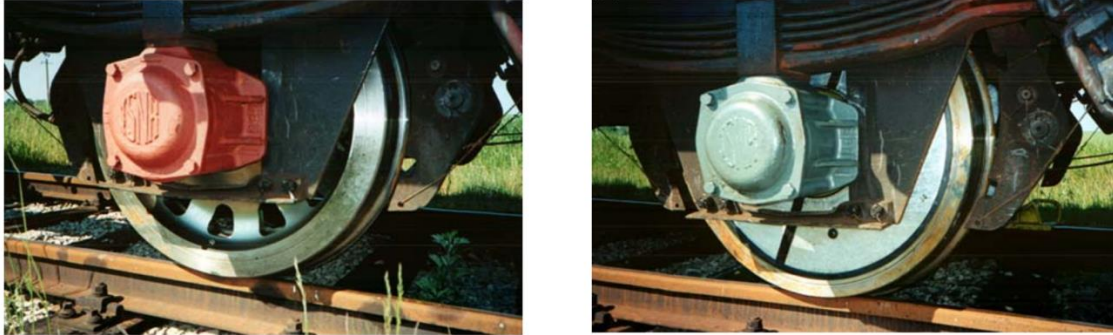
Figure 4. Prototype designs tested in the work reviewed in [19]. Prototype of a perforated wheel (a) and of profile-optimised wheel design (b).

Other noise sources:

Although the predominant source is rolling noise, the following are other noise sources briefly described in order to account for their physical phenomena. These physical phenomena are of secondary importance due to either the fact that their A-weighted noise power level contribution is low or either the fact that there occurrence is less frequent and is given only in some occasions (like squeal noise or bridge noise).

Aerodynamic noise in trains is mainly caused by turbulent airflow phenomena through the train components, especially through the bogie's wheelsets. Due to the high speeds of modern trains, aerodynamic noise has become an important contribution of overall noise production, especially at speeds over 300km/h [21].

Squeal noise is either produced in curves (curve squeal noise) or during braking (brake squeal) and is a kind of noise whose energy is highly concentrated in a narrow band of the frequency domain, also called tonal noise. This tonal noise is related with one of the eigenfrequencies of the wheel which is excited by intermittent transverse forces during curving.

Bridge noise is another type of secondary source. Forces acting from the track to the bridge when a train runs over a bridge produce its excitation resulting in noise emissions that can reach values of 20dB in the low frequency range, and that have a great dependence on the type of bridge.

Ground-borne noise and vibration from railway lines can cause human distress/annoyance, and also negatively affect real estate property values in tunnel metro operations, urban trams and exterior railway lines [22]. This source of noise is very complicated to control and predict, due to the non-uniform propagation medium.

Other sources include noise from mechanical components (such as the engine and exhausts or intakes of diesel engines), warning signals or shunting noise, between others.

2.2   Acoustic Power Calculation

2.2.1   Overview

In order to carry out an optimization process to minimize the amount of radiated sound power by the wheels, it is crucial to have a numerical relationship between the sound power and input (candidate) geometry. In the following top-to-bottom mathematical description, first the final equations are stated to show the required unknowns which are solved step-by-step to finally reach the candidate geometry input variable. The process is graphically explained in Figure 5 to easily visualize how the input wheel design produces a certain radiated acoustic power distribution.
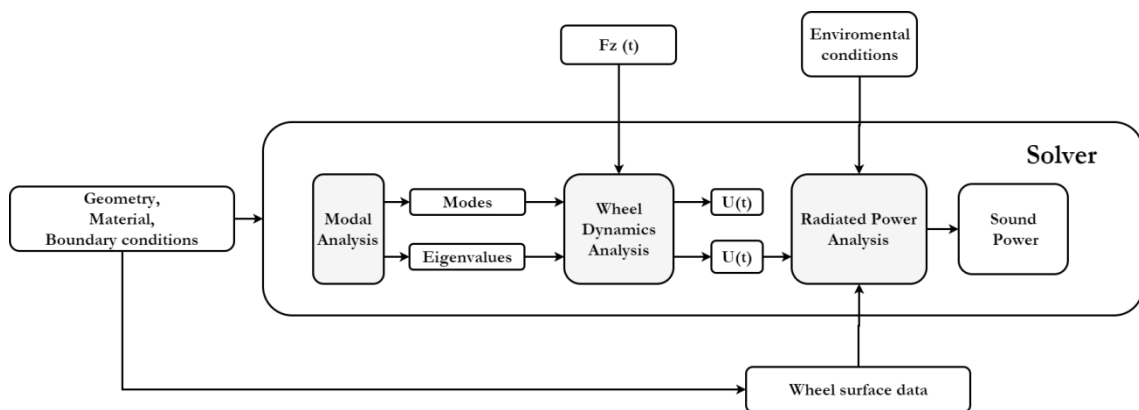

Figure 5. Simplified Block diagram showing the basic procedure used to calculate acoustic sound power from railway wheels. A more rigorous version of this diagram is shown later on.

2.2.2 Equations

From velocity to sound power

Intuitively, we can imagine the acoustic model of the wheel as a percussion instrument, similar to a drum. It can easily be proven that if the drum web vibrates more energetically, a louder sound is created. This is the same as stating that the velocity (or kinetic energy) of the drum web is proportional to its radiated sound power. In our wheel analogy, this phenomenon also occurs.

$P_{3/8}^i$, the acoustic power radiated (in dB) by the surface i in a certain third octave of the frequency spectrum, is related with the speed of the nodes of the wheel's web according to the following equation:

$$P_{3/8}^i = \sigma \cdot \rho_a \cdot c_o \cdot \left(v_{S,3/8}^i\right)^2 \cdot S^i \tag{4}$$

Where

- ρ_a is the density of air, which is taken to be ρ_a = 1.20 kg/m³.
- c_o is the speed of sound in air, with value c_o =343m/s².
- $v_{S,3/8}^i$ is the effective speed of the surface i , in a certain third octave band.
- S^i is the surface area of surface i .
- σ is the radiation efficiency. As discussed later, in this work the radiation efficiencies are not considered due to the analysis complexity and computational cost associated with its calculation, so it is considered that $\sigma = 1$ in all cases

Considering vector notation for all i surfaces in the vibrating 'skin' of the wheel we obtain the following equation:

$$\{P_{3/8}\} = \sigma \cdot \rho_a \cdot c_o \cdot \{v_{S,3/8}\} \circ \{v_{S,3/8}\} \circ \{S\} \tag{5}$$

Being ∘ the Hadamard dot product.

From the vibrational response to velocity

To calculate the velocity of a railway wheel caused by some vibration phenomenon, it is first required to understand such phenomenon. The vibration response of the wheel will be affected by the natural vibrational response of the wheel system and the force acting on such system.

The natural vibrational characteristics of the wheel are expressed by its natural frequencies (also called eigenfrequencies) and its modal displacements. Natural frequencies are expressed using the vector of the first m eigenfrequencies, $\{\omega_n\}$, where m is the minimum value so that the highest calculated eigenfrequency is 5000Hz. This 5 KHz limit is the taken upper frequency limit to analyse, as radiated sound in higher frequencies can be ignored due to the reduced sensibility of the human earing system in these levels. The modal displacements matrix $[\Phi]$ contains information about how the system vibrates.

Once $\{\omega_n\}$ and $[\Phi]$ are obtained, the speed matrix in modal coordinates $[v_{mod}]$ can be calculated by solving the following differential equation:

$$[M_{mod}][\ddot{q}] + [K_{mod}][q] = [Q_{mod}] \tag{6}$$

Where $[K_{mod}]$ and $[M_{mod}]$ are the stiffness and mass modal matrices, respectively, and are obtained by:

$$[M_{mod}]_{mxm} = [I]_{mxm} \tag{7}$$
$$[K_{mod}]_{ii} = \omega_{n,i}{}^2 \; ; \; K_{ij} = 0 \; for \, i \neq j \tag{8}$$

And $[Q_{mod}]$ is the modal force calculated using the time-domain contact force $\{F\}$ (which is later explained) with the following expression:

$$[Q_{mod}] = [\Phi]\{F\} \tag{9}$$

Once the dynamics of the system is calculated, the modal velocity vector is determined by:

$$[v_{mod}] = [\dot{q}] \tag{10}$$

Once the speed matrix in modal coordinates $[v_{mod}]$ is obtained, the speed matrix of each 3 DoF of a surface node j expressed in physical coordinates in the time domain is obtained my multiplying $[v_{mod}]$ with the modal displacement matrix.

$$[v_{N,phys}^{j}] = [\Phi^{j}][v_{mod}] \tag{11}$$

Where $[\Phi^{j}]$ is a matrix containing the modal displacements of surface node j. Only surface nodes are used, as these correspond to the wheel's radiating surface elements. Then, to obtain a vector containing the velocities for each surface $\{v_{S,phys}\}$, the nodal speeds in physical coordinates are averaged and projected to their normal components.

In order to get a better visualization of the frequency content of the velocities (and ultimately, of the acoustic power response), the surface velocity vector is transformed from time domain to frequency domain using the Fourier transformation. Finally, and once the surface velocity vector is in the frequency domain, we can discretize the velocities into third octave bandwidth groups, obtaining $\{v_{S,3/8}\}$.

In this work, the effect of damping is not considered due to simplicity of analysis and reduction of computation time and due to the fact that the energy absorbing capacity of a railway wheel is low. According to [3], the system is dominated by eigenfrequencies and so, we can make this assumption with relatively precise results.

From the geometric input to the vibrational characteristics of the system

The natural vibrational characteristics of the wheel can be calculated using modal analysis with the help of a Finite Element (FE) software, and requires the definition of a FE mesh, and the corresponding boundary conditions. The expressions for these are shown in Equation 12 and 13.

$$det\big[[K] + \lambda^2 [M]\big] = 0 \tag{12}$$
$$\lambda^2 = \pm i\omega_n^r, \quad r = 1, \dots, m \tag{13}$$

Where ω_n^r is the eigenfrequency, (or natural frequency) of the vibration mode r. $[K]$ and $[M]$ are the stiffness and mass matrices in physical coordinates which depend of the geometry, of material properties and boundary conditions, and are calculated in this work using ANSYS APDL. Once the natural frequency vector is obtained, we can calculate the mode of vibration r with the following equation:

$$([K] - \omega_n^r [M]) \{\Phi^r\} = 0 \tag{14}$$

The vector $\{\Phi^r\}$ contains the modal displacements of the wheel of the mode r.

The FE mesh contains the discretized geometrical data of a candidate wheel design. It is described using two variables: the nodal coordinates and the topology matrix. The nodal coordinates contain the Cartesian XYZ positions of the nodes which form the mesh, and the topology matrix contains the nodes attached to each of the 3D elements used. These variables are obtained using ANSYS software, which creates a FE mesh from a certain input- geometrical description. This geometric description is the input candidate design. Finally, in order to create the mesh, we introduce the material properties described in Table 2.

2.3 Structural Analysis

2.3.1 Overview

A realistic optimum acoustic design must also meet the usual resistance of materials criteria; therefore during optimization the candidate designs which do not meet these resistance standards are filtered. Only structurally valid ones are accepted and to evaluate the structural resistance of the wheel, a high-cycle fatigue analysis of each candidate design is considered.

2.3.2 Application

To assess the mechanical resistance of a candidate design wheel a FE fatigue analysis was carried out through the FE software ANSYS APDL. After selecting the wheel material properties (Table 2) and creating a mesh from the proposed geometry, we set the Dirichlet boundary conditions through the axle displacement constraint (considering it to be built-in), and the Neumann boundary conditions, which in this case was elected to be a uniform nominal Hertzian pressure along all the possible contact areas.

By applying the Hertzian pressure in all areas we assure that the wheel is evaluated in all 360 degrees of rolling, and therefore in any potentially weak points caused by any perforation design combination. Of course, applying pressure at whole surface of the wheel (not only over the contact area) is a conservative approach.

The nominal Hertizan contact pressure p_n was calculated assuming a cylinder-to-elastic half space contact. The pressure distribution for this case is given by Equation 15 and obtained from [23].

$$p(r) = p_0 \left(1 - \frac{r^2}{a^2}\right)^{-0,5} \tag{15}$$

$$p_0 = \frac{1}{\pi} E^* \frac{d}{a} \tag{16}$$

Where p_0 is the maximum pressure from the Hertzian pressure distribution (obtained by Equation 16), r is the contact domain and a is the radius of the indented surface area of depth d. E^* is the equivalent Young Modulus and is obtained with the wheel and rail material properties using Equation 19. While a is estimated as the length of the wheel contact line, d is obtained through Equation 17 which relates this parameter with the known force F.

$$d = \frac{F}{2RE} \qquad (17)$$

$$a = \sqrt{Rd} \qquad (18)$$

$$\frac{1}{E^*} = \frac{1-v_w^2}{E_w} - \frac{1-v_R^2}{E_R} \qquad (19)$$

p_n, the nominal pressure acting on the indented surface in the wheel /rail contact as a cause of a force F, can be estimated by integrating Equation 15 in the domain created by the calculated contact surface area, of radius a (Equation 18). p_n is defined in Equation 20.

$$p_n = \int_a^{-a} p(r) \, dr \qquad (20)$$

Evaluating Equation 17 with the force F_m being the mean force and with the force F_a being the alternating force we finally obtain $p_{n,a}$ and $p_{n,m}$ corresponding to the mean and alternating Hertzian pressures. These values are then combined as two load cases in ANSYS APDL to obtain the maximum von Misses tension in all nodes $(max[(VMT)_n])$ through a Soderberg static equivalent stress method. For this method, the constants to calculate the fatigue limit S_e where set so that $\frac{S_y}{S_e}$ was 2,07.

Material properties					
Property	Type	E [GPa]	S_y [MPa]	v	ρ [kg/m³]
Wheel Material	UIC 812-3 R6 T,E	210	400	0,3	7850
Rail Material	UIC60	210	400	0,3	7850

Table 2. Material Properties of the wheel and rail in the analysis.

Hertz parameters and results	
L	2
R	2
F_a	46,21 kN
F_m	74,72 kN
$p_{n,a}$	1,16 MPa
$p_{n,m}$	1,87 MPa

Table 3. Parameters and results related to the fatigue analysis done. F_a and F_m are obtained from the dynamic force record described later in this work.

2.3.3 Evaluation

The model is structurally acceptable if the maximum von Misses tension (VMT) is not greater than the yield strength of the material used. The above explained is summarized in the following equation:

$$max[(VMT)_n] < S_y \qquad (21)$$

Where $max[(VMT)_n]$ is the maximum von Misses tension from all the set of n calculated nodes.

3 Analysis Model

3.1 Overview

It is considered that a FE model of an axially-attached railway wheel is excited from a vertical dynamic force, and that the acoustic emission from the wheel is proportional to the normal velocities of the wheel surface elements.

3.2 Boundary Conditions

3.2.1 Dirichlet Conditions

In the real wheel-bogie-rail system, the wheel is translationally constrained in all the axes (XYZ) as a cause of the axle-mounted components and the rail vertical contact. To simulate these, the FE wheel model is totally constrained (built-in) in its axle contact, as shown in Figure 7 (c) and (d). Although in the real system there is no wheel-axle rotational constraint, for the purpose of the acoustic analysis we consider the wheel and axle to be the same elements and therefore to hypothetically rotate together (but only for constraint condition issues).

3.2.2 Neumann conditions

The force input was modelled differently for each objective. The first one, to calculate fatigue stresses. The second one, to provide an excitation for the acoustic analysis.

For the former, a surface Hertzian pressure is applied to test the structural resistance of the wheel to high-cycle fatigue. Basically, the mean and alternating pressures on areas were imposed through a combined load case. These mean and alternating pressures (mathematically described in Section 2.3.2) were obtained from the mean and alternating forces obtained from the force record.

For the latter objective, the force record is applied in the contact point, as an excitation for the system in order to calculate the radiated power. The record is the result of the time-wise interaction between the wheel and rail roughness and the reaction force on the wheel caused by the part of the total train weight acting on the wheel. The dynamic force record (shown in Figure 6) was obtained using the pseudorandom rail roughness specified in the ISO3095 regulation [24]. This force is applied on the normal direction of the contact surface node (which is taken to be the direction on the vertical axis Y from the Cartesian coordinate system shown in Figure 7 (a). According to literature, the contact node is located at 7cm towards the interior of the wheel.
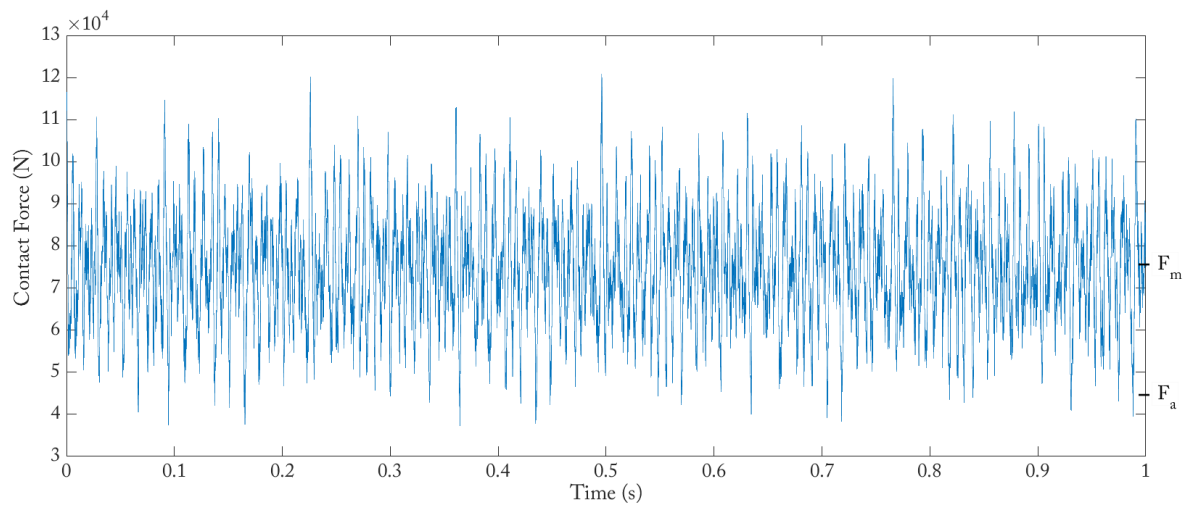
Figure 6. Force time record used in the analysis and obtained from the pseudorandom roughness specified in [24].
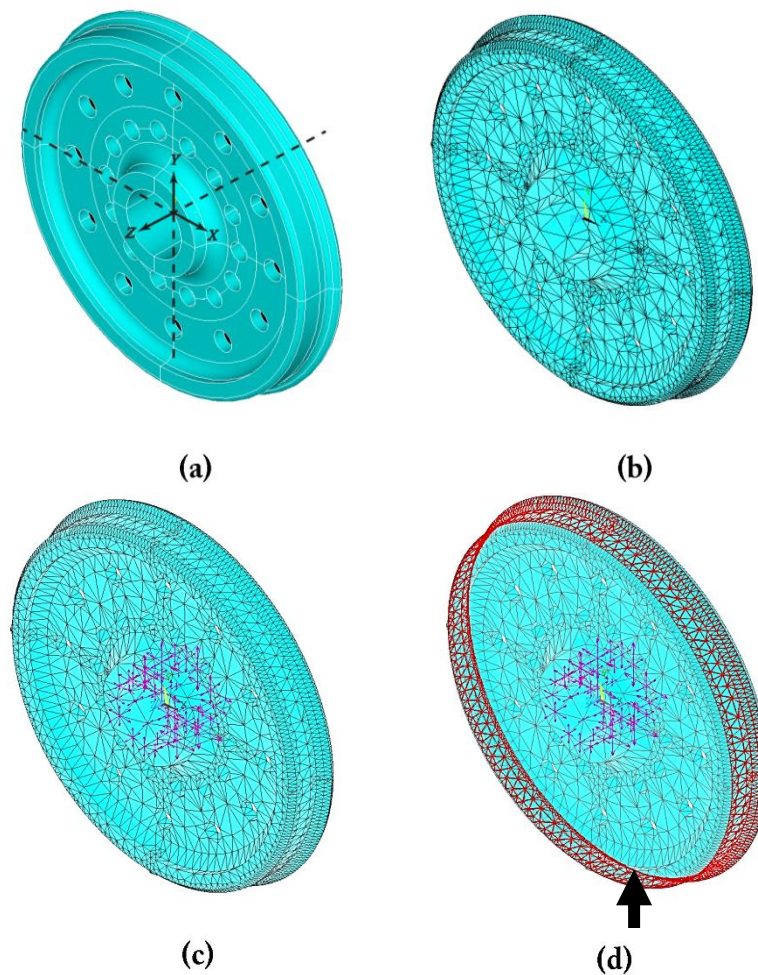
Figure 7. (a) Starting volume of an arbitrary example of perforated wheel. (b) Meshed volume. (c) Displacement constraint (magenta) conditions for the modal analysis. (d) Nominal pressure load (red surface) for structural analysis, contact point force for acoustic power analysis (black arrow) and displacement constraint (magenta arrows) conditions for the fatigue analysis.

3.2.3   Environment conditions.

In order to calculate the acoustic power, the air conditions are set so that the density of air, ρ_a, is 1.20 kg/m³ and c_o, the speed of sound in air, has a value of c_o =343m/s².

3.3   Assumptions.

3.3.1   Radiation efficiencies

The acoustic radiation efficiency σ is a term often used in literature [3], [25] to quantify the capacity of acoustic power radiation a component due to changes in its physical properties (like for example, changes in its geometry), relative to a certain reference. In this case, the radiation efficiency is the acoustic power radiated as a cause of the vibrational characteristics of the analysed wheel (with its changes in geometry) as compared to the radiation of a totally flat and solid disk. In the case of a perforated wheel, the type of geometry modification considered in this work, the radiation efficiency will be possibly reduced compared to that of a unperforated wheel, as suggested in literature based on the 'acoustic short-circuiting' effect [3].

The calculation of the radiation efficiency of a particular geometry requires a deep and complex analysis and a vast computational cost, and being this work a preliminary study, this complex is not considered. The radiation efficiency through web perforation is estimated to be highly influential on the final result, so this assumption is a critical point to improve for future improvements in this research area.

3.3.2   FE discretization errors

In order to obtain an adequate precision in the FE analysis performed, the FE mesh discretization must provide sufficient calculation nodes in order to represent small changes in geometry which can affect vibrational characteristics and therefore the final result. Due to the relatively high computational cost of optimization through an iterative analysis, a mid-term between precision refinement and computation time was targeted in mesh creation.

3.4   The unperforated wheel

The unperforated wheel taken as a starting point was created from typical wheel dimensions. It is based on a monobloc AAR M-107/M-208 standard specification, slightly modified in order to simplify the model for a lower computational cost. Figure 8 shows different views from the unperforated wheel and its general dimensions.
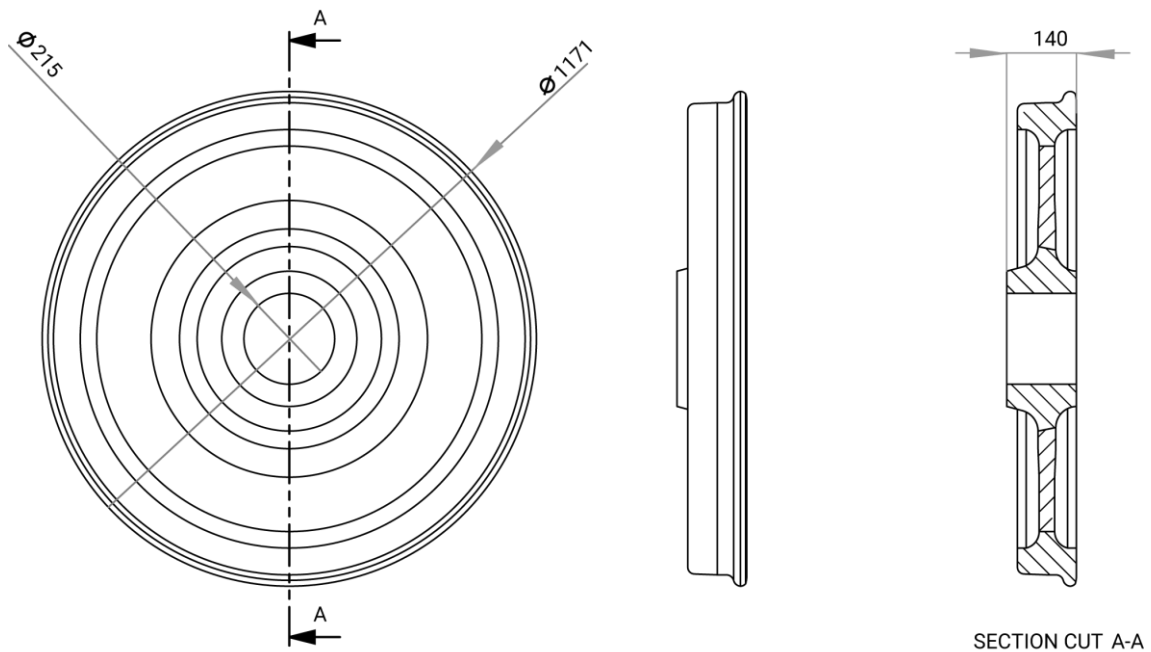
Figure 8. Different views from the unperforated wheel and general dimensions. A detailed version of this drawing is offered in Annex III (III.1) with measurements.

As it can be seen in Figure 8, the web profile is almost completely straight. The use of a straight web profile is advantageous, as it simplifies the geometric model, reducing computational cost. However, the fact that a straight web profile has low radial and axial motion coupling can in fact produce reduced acoustic power levels, making it potentially more difficult to document sound minimization.

4. The Optimization Loop

This chapter describes the data flow mechanism which was developed for the minimization of the acoustic radiation of railway wheels.

4.1 Introduction

In an optimization loop, a large amount of iterations are required to achieve an optimum design. Computing this amount of iterations individually, by manually sending data through the task modules, is not the desired approach. In order to create a robust optimization loop, which acts as an automatized black box process, a series of task modules need to be computationally connected, creating a closed information flow which permits a relatively big amount of iterations in a relatively low amount of time.

To create this closed loop, there are three main modules used: a mesher, a solver and an optimizer. As a central commander module, Matlab is used. Through this software, ANSYS was launched through batch mode, and its output data files are arranged to suit the solver routine which provided another data files then fed to the optimizer (which was a Matlab sub-routine). A simplified block diagram of the optimization loop is shown in Figure 9 while the whole optimization loop is shown in Figure 10.
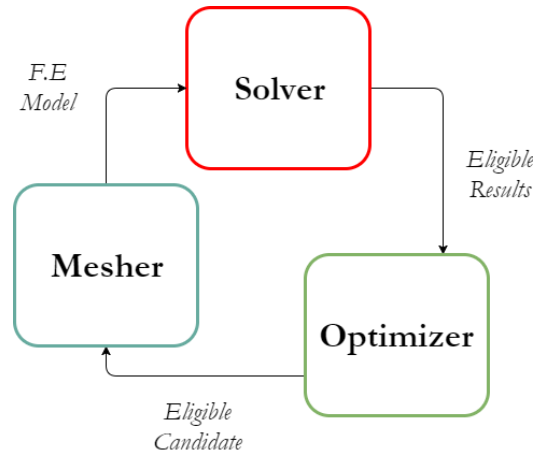
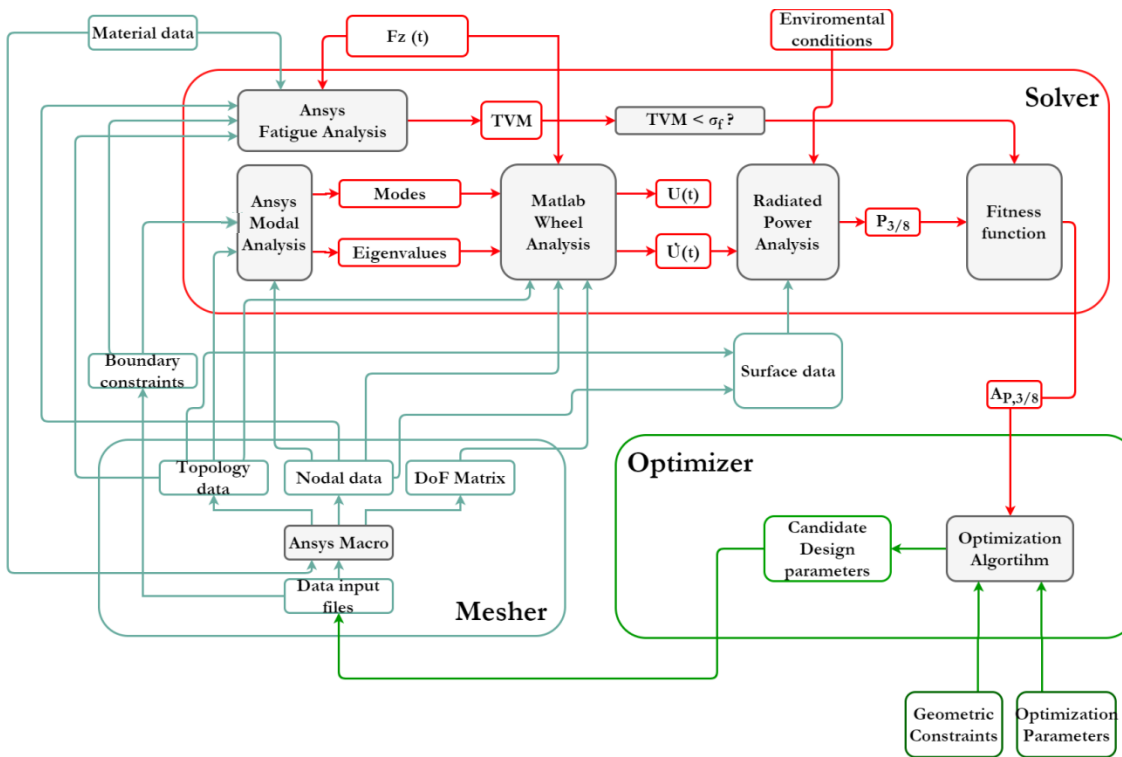*Figure 9. Simplified block diagram summarizing the main modules of the optimization loop.*

Figure 10. General block diagram showing a more detailed optimization loop.

4.2   Mesher

Due to the scale of complexity of the problem in hand, FE analyses were used for the modal, stress and sound power analyses. A discretized FE mesh is needed, which is composed from a parametrized design. In this case, ANSYS was used to create the FE mesh through a parametrized macro file due to the flexibility and options available of the software. The macro file has the necessary data to produce the candidate geometry according to specific design variables. For the problem at hand, 10-node tetrahedral elements are used.

The finite element mesh is composed by three data files, the topology data file containing the nodes shared by each element, the nodal data file containing the Cartesian (xyz) coordinates of the nodes, and Degrees of Freedom (DoF) data file which contains the ordered indices of each of the 3 DoF by each node. The mesher was also used to obtain the surface elements of the candidate wheel, needed for sound power calculation. The reader is referred to Figure 10 for a better comprehension.

4.3   Solver

The solver module processes the problem data (FE mesh, boundary data, material data and external forces) to produce numeric evaluations of the objective function used in the optimization process. More precisely, the solver module was used to perform a modal analysis, to extract the free vibration modes and eigenvalues as explained in Section 2.2.2, which were then used to obtain the wheel dynamics (Equation 6) necessary to calculate the three-octave dB(A) profile of radiated acoustic power (Equation 4).   In addition, a fatigue structural analysis is carried out to obtain the maximum Von Misses Tension $max[(VMT)_n]$ in order to filter those candidates which do not satisfy the material resistance constrains. This process is illustrated in Figure 10.

4.4   Optimizer

The optimizer module is fed by the relevant result obtained by the solver module, which is the evaluated objective function. In the Approach 1 strategy, the objective function is the area below the three-octave dB(A) profile of radiated acoustic power, or $A_{p,3/8}$. The goal of the optimizer is to generate a design candidate such that its acoustic power emission intensity is minimum (i.e to minimize $A_{p,3/8}$). To do so, the optimizer is based on an optimization algorithm which learns from previous solver inputs, in an improving strategy which will, after a number of iterations, find an optimal geometric design. The recursive candidate designs generated by the optimizer are fed to the mesher, which will then produce the corresponding FE mesh, closing the total optimization loop. This design improving strategy will depend on the type of algorithm used and on the parameters which tune the operation of such algorithm.

4.4.1 Parametrization

In order to extensively test how the design of a web perforation scheme affects the radiated sound power, we need to provide to the optimization algorithm enough freedom to explore a sufficiently large design space. This freedom is defined by the number of design variables, their discretization and their lower and upper bounds.

As shown in Figure 11, the perforation scheme is parametrized into rows r of perforations, each one having three design variables, namely: X_r, the distance to the wheel's centre of row r, R_r, the radius of the perforations in that row and N_r, the number of perforations in that row. 3-row, 2-row and 1-row optimizations were launched separately. The upper and lower bounds of design variables were decided by the geometric constraints due to the design space considered (the web of the wheel), manufacturing limitations and inertial considerations (radial symmetry with a pair number of perforations). The discretization of the search space is constrained by the computational cost, as a very refined discretization will force a very refined exploration with many candidates to analyse.

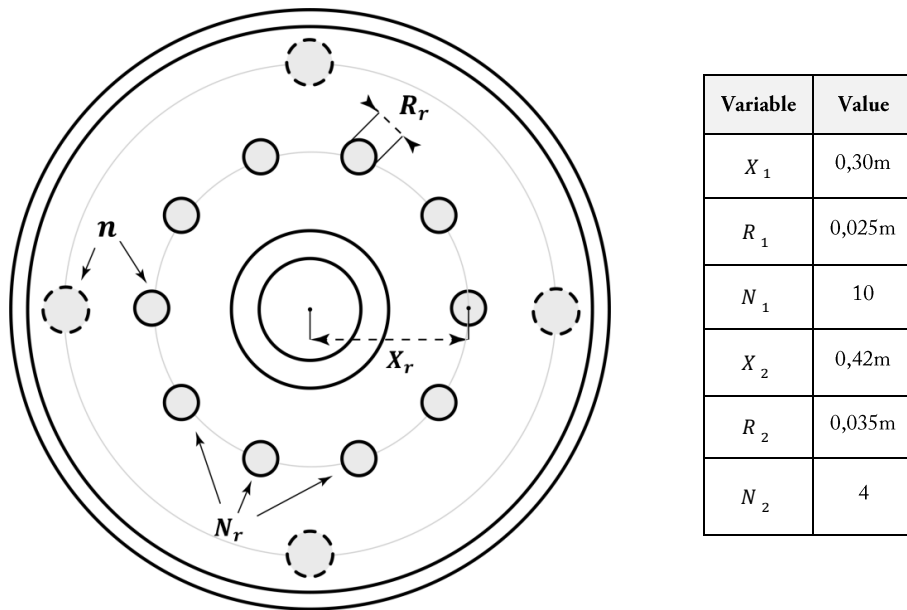| Variable	Value
X_1	0,30m
R_1	0,025m
N_1	10
X_2	0,42m
R_2	0,035m
N_2	4

Figure 11. Illustration of the parametrization scheme used for an arbitrary design example. In this case, as n is 2 (there are 2 rows), there are 6 different variables that define the perforation scheme which are shown in the table.

4.4.1.1 Parameter bounds and optimization strategies

For each row optimization, different row-specific bounds where made to adequately cover all the web space, these are shown in Tables 4-6. Discretization was adjusted specifically to the optimization approach as seen later on.

Two types of optimization strategies were done in order to search for better optima. In one, we impose the number of perforation rows to the Genetic Algorithm (GA), focusing the search. In the other one, called here 'n-row optimization', we add the number of rows n as one more parameter to be optimized by the GA. Of course, as seen later, this strategy is computationally expensive and should provide similar results when performed many times (due to the stochastic nature of GA's). Nevertheless, the n-row optimizations were done to widen the result spectrum, in order to enrich the study.

Variable	Lower Boundary	Upper Boundary
X_1	0,2m	0,3m
R_1	0,025m	0,04m
N_1	2	16
X_2	0,3m	0,4m
R_2	0,025m	0,04m
N_2	2	16
X_3	0,4m	0,45m
R_3	0,025m	0,04m
N_3	2	16

Table 4. Boundaries for a 3-row parametrization.

Variable	Lower Boundary	Upper Boundary
X_1	0,2m	0,35m
R_1	0,02m	0,04m
N_1	2	16
X_2	0,35m	0,45m
R_2	0,025m	0,04m
N_2	2	16

Table 5. Boundaries for a 2-row parametrization

Variable	Lower Boundary	Upper Boundary
X_1	0,2m	0,45m
R_1	0,02m	0,045m
N_1	2	16

Table 6. Boundaries for a 1-row parametrization.

4.4.2   Genetic Algorithm

A GA was used as the optimization algorithm. These algorithms are particularly interesting as they use mathematical procedures which emulate the evolution of species in order to iteratively improve design candidates [26]. As compared to deterministic optimization algorithms, they only require an objective function evaluation in order to optimize design variables and they have proven to be very effective in problems with vast and complex (non-linear, non-continuous) design-objective-function relationships. As an example, in [10], GA where used to minimize sound radiation from railway wheels through the web profile modification.

In this research, the GA used was the one integrated in Matlab. This GA can operate with user-defined parameters like the population size, maximum number of generations, crossover, mutation, elitism... The options modified for the present work were mainly the first two from the listed and are explained below.

- *Design Candidate:* A candidate is a coded design, which in this research corresponds to the set of parameters (Figure 11) which define the perforated scheme of the wheel, and through the function evaluation, its radiation characteristics.

- *Maximum Generations:* Usually, during a generation candidates are evaluated and selected based on their fitness value.   It is used as one of the stop-criterions, as if this number is reached the genetic algorithm will return the best candidate found and the optimization loop will stop. A higher generation limit will usually increase the probabilities of improving the population's genetics (at the expense of more computations), but in some cases early generations can find a relative global optimum design and the remaining generations will be stuck in this one, thus can be unnecessary. For extreme cases, a second stop criterion is used, which is that the objective function remains un-improved for a certain number of generations.

- *Population Size:* The number of design candidates generated in each generation. A higher population will increase the chances of finding valuable design information for future generations, but will increase computation cost as more candidates are evaluated.

As GA is a stochastic optimization process, different optimization Loops were tested with different GA tunings, mainly by changing the Population Size and the Maximum Generations in order to observe what conditions derived to the best optimum candidates and with what computational expense.

4.4.3 Solver approaches

Two different solver approaches were created in order to analyse the performance of optimization methodologies with different computational cost. Both methodologies are designed to minimize acoustic radiation, but while Approach 1 is a direct minimization and thus, requires the calculation of radiated noise, Approach 2 is an indirect one and only requires a modal analysis. A comparison of both approaches is explained in Figure 12(a) and 12 (b).
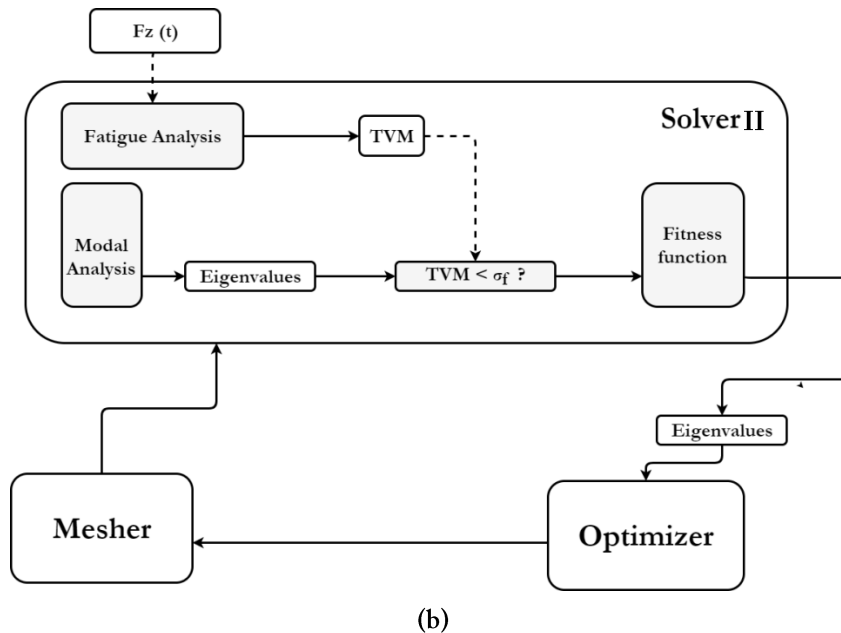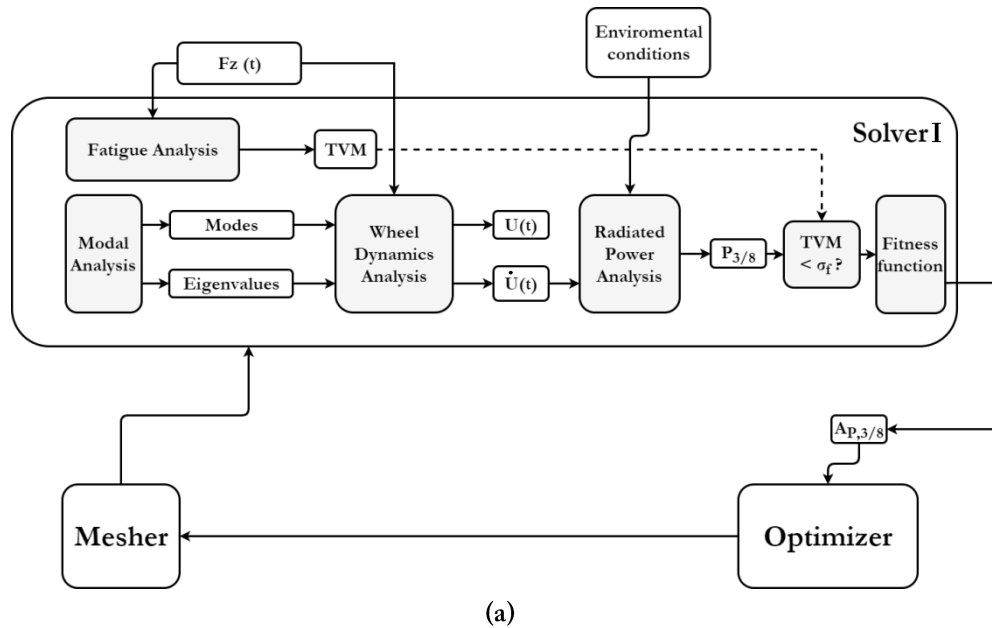

(a)

(b)

Figure 12. (a) Solver used in Approach 1 connected to the (simplified) Mesher and Optimizer. (b) Solver used in Approach 2. It can be clearly seen that Approach 2 only a small part of the Solver in Approach 1 is required.

For this approach Equations 4-13 are used to calculate noise radiation at a discrete number of frequencies as explained in chapter 2, this provides a direct objective function to the GA optimizing algorithm, which will eventually search for improved (more silent) candidates.

This objective function is the sum of calculated dB(A) radiation power in each frequency, which is basically the sum of areas of rectangles created when discretizing the frequency domain in third octaves and named $A_{P,3/8}$.

Approach 2: Maximization of Eigenfrequencies

As explained in chapter 2, increasing the natural frequencies of the wheel can reduce noise radiation, as also shown in literature [22]. This is due to the fact that by alienating the natural response of the system from the excitation frequency range (1kHz to 5kHz), the acoustic emission will decrease in this rank.

In this case, the solver required to feed the GA optimizer is far less expensive, as only a modal analysis, mathematically described in chapter 2, is needed to extract the eigenfrequencies. The modal analysis used in this approach is identical to the one used in Approach 1, however in Approach 2, a modal analysis upper limit of 7kHz was set (until which the analysis extract modes) to allow the frequencies to grow further than 5kHz. The objective function in Approach 2 was the inverse of the mean natural frequency, named $\omega_{n,obj}$.

This approach is indirect as the optimizer does not necessarily minimize radiation levels. Once the optimum has been found, its $A_{P,3/8}$ is calculated, in order to know its acoustic properties towards comparison.

4.4.4 Computational hardware.

The optimization processes were computed using a server unit with the following characteristics:

- CPU: Intel® Xeon® ES430 @ 2.66GHz dual core.
- RAM: 32Gb
- OS: Windows server 2012 r2.

In order to reduce computational times a second unit was also used in parallel. The computation times described in the next section refer to the use of these computation units.

5 Results

5.1 Introduction

In order to evaluate the results obtained, first the unperforated-wheel noise radiation levels are calculated using the model proposed Section 2.2.2 which is also used to calculate noise radiation from perforated wheels. Thus, in this chapter first the results for the unperforated (base design) wheel are described. Its dB(A) noise radiation spectrum in the frequency domain (discretized in third octaves) is shown (Figure 14). Along with this, the sum of areas below the acoustic power curve, $A_{P,3/8}$, the structural simulation results and a qualitative analysis of the most relevant modes of vibration, are specified.
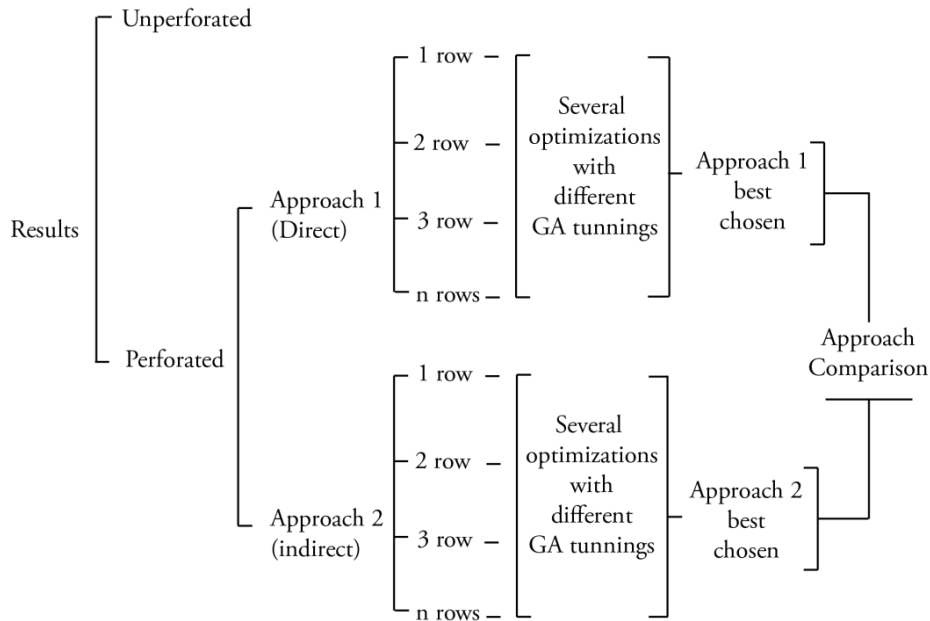

Figure 13. Organization of results.

Once the acoustic results of the standard wheel have been described and commented, the improved results with wheel perforations are shown. These are divided in Approach 1 results, and Approach 2 results, following the methods explained in chapter 2 and 3. Each approach contains 3 different optimization loop results, each one created with a different GA tuning, plus an n-row optimization where the number of perforation rows is an additional variable to optimize. For each approach, the results are discussed and a comment on the effect of GA parameters is made. Finally, an overall comparison of the two approaches is made. A summary of how the results are organized and the content in each of this chapter's parts is illustrated in Figure 13 for a better comprehension of the reader.

5.2   Unperforated wheel results

5.2.1   Acoustic power curve.

The calculated noise radiation spectrum in dB(A) scale is shown in Figure 14, along with the sum of areas below the curve, $A_{P,3/8}$. In this case, to reach a 5kHz analysis window, $m=49$ number of modes were calculated. As explained before, the number of modes calculated is not a fixed value as it is the modal analysis algorithm (in ANSYS) which 'decides' how many modes to extract to reach 5KHz.

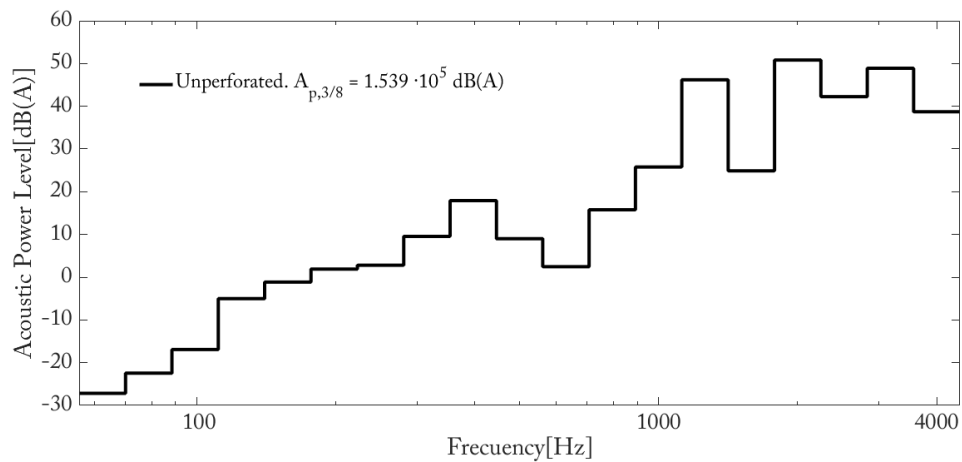*Figure 14. dB(A) acoustic power level of an unperforated wheel in the 50–5039Hz range.*

5.2.2   Mode Analysis

In the following page, we describe the modes of vibration which share the highest amount of radiated noise. Identifying the most influential ones is crucial when comparing results of perforated wheels, as if they radiate less noise, they will probably reduce their maximum axial displacement in those critical modes.

Max. Displacement
0.088m

Max. Displacement
0.079m

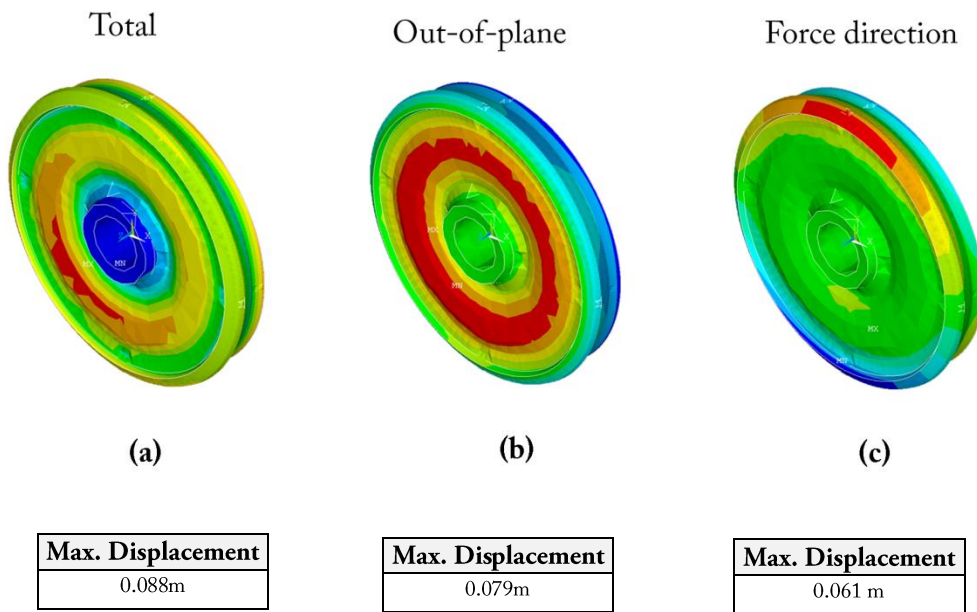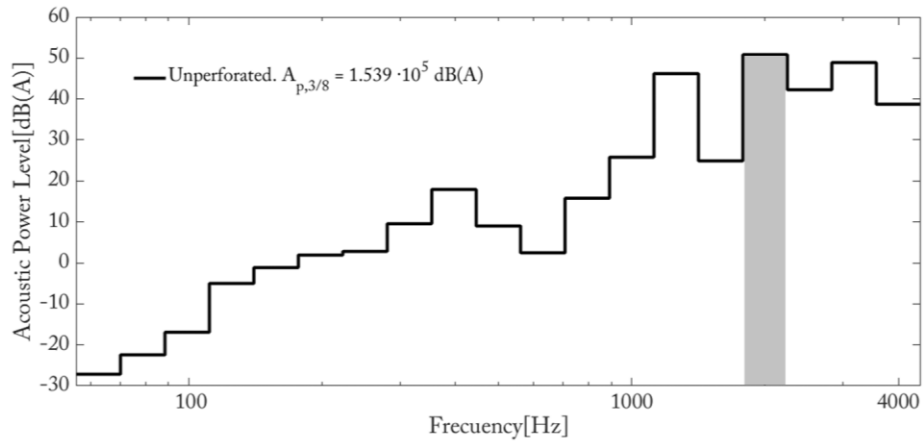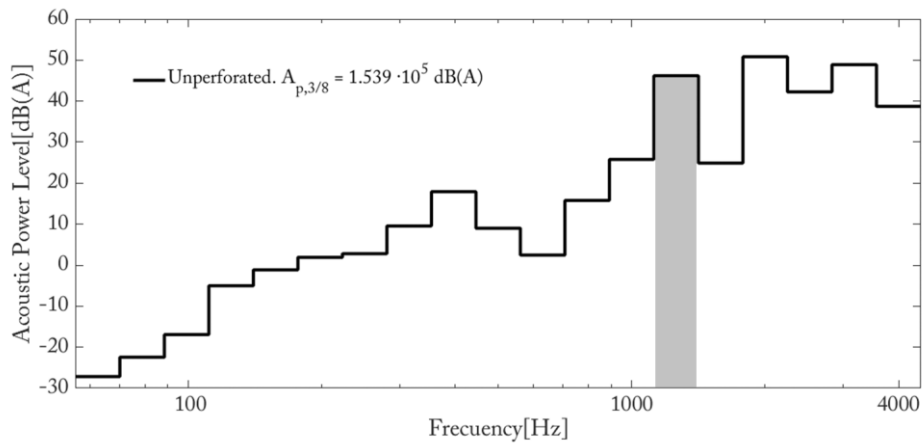| Max. Displacement |
|---|
| 0.061 m |

Figure 15. Modal displacements at the 2106Hz mode for an unperforated wheel. (a) shows the total (sum), (b) the out-of-plane (Z axis, or axial direction) and (c) force direction (Y-axis, or vertical direction). Note that the colour scale is relative to each result and is shown for a qualitative description. Click here to watch the corresponding animation for this mode (only for the CD format).

Figure 15 shows an 'umbrella-opening-like' mode of vibration which intuitively can be identified as a very relevant mode due to its similarity to a loudspeaker's movement. This mode is the one with the highest radiation peak. The apparent reason for this is that, although this mode is not highly excited by the contact forces (which are have a purely vertical component), it is a vibration mode which naturally is prone to axially radiate noise and even a slight excitation in an almost plane wheel creates the sufficient coupling for a very high radiation as the one calculated.
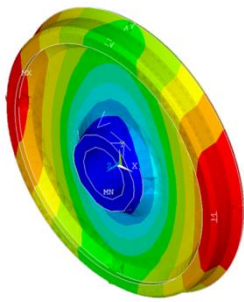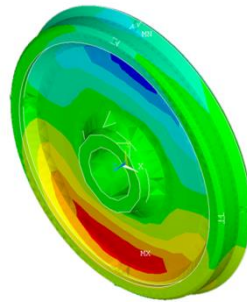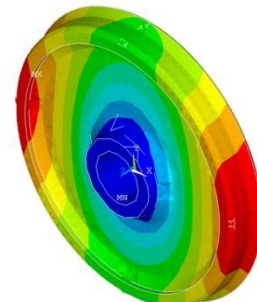
Max. Displacement
0.0673m

Max. Displacement
0.003m

Max. Displacement
0.06728 m

Figure 16, Modal displacements at the 1247 Hz mode for an unperforated wheel. (a) shows the Total (sum), (b) the out-of-plane (Z axis, or axial direction) and (c) force direction (Y-axis, or vertical direction). Note that the colour scale is relative to each result and is shown for a qualitative description. Click here to watch the corresponding animation for this mode (only for the CD format).

Figure 16 shows a mode of vibration mainly on the vertical Y axis. It is easily seen how this mode is prone to be excited by a Y-axis orientated force. As opposed to the mode of vibration shown in Figure 15 the displacement shown in this mode is predominantly vertically orientated and therefore should not produce a high noise radiation unless the excitation shared a very similar frequency content and direction with it, possibly what is actually happening.

Max. Displacement
0.099m

Max. Displacement
0.097m

Max. Displacement
0.02 m
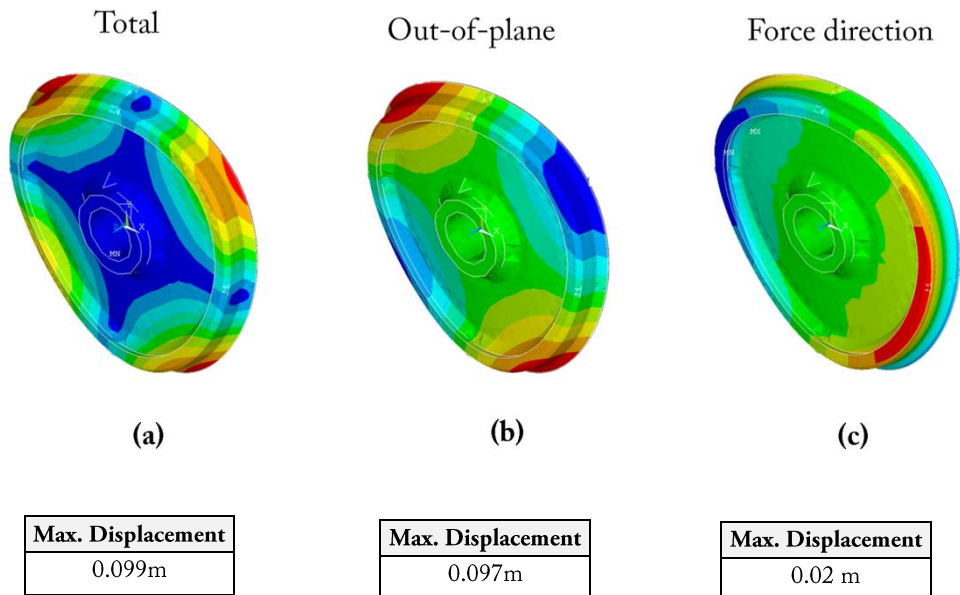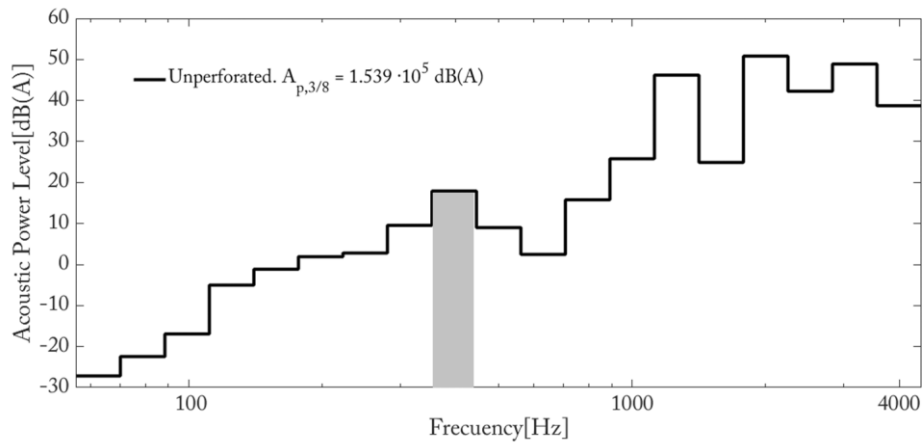
Figure 17, modal displacements at the 428 Hz mode for an unperforated wheel. (a) shows the total (sum), (b) the out-of-plane (Z axis, or axial direction) and (c) force direction (Y-axis, or vertical direction). Note that the colour scale is relative to each result and is shown for a qualitative description. Click here to watch the corresponding animation for this mode (only for the CD format).

Figure 17 can roughly be described as a hybrid of the phenomena shown in Figures 15 and 16, as it has a kind of axial displacement while having also a component of Y-axis displacement.

5.2.3   Stress Analysis

Figure 18 shows the von Misses criteria-based stress distribution as a cause of applying the method described in section 2.3, as well as the safety factor X. As it can be seen, an adequate level of $X_{unp} = 11.4$ with a maximum of 36MPa shows a high degree of resistance of the unperforated wheel, which leaves a relatively safe margin towards perforation.

0.27 Mpa   36 Mpa
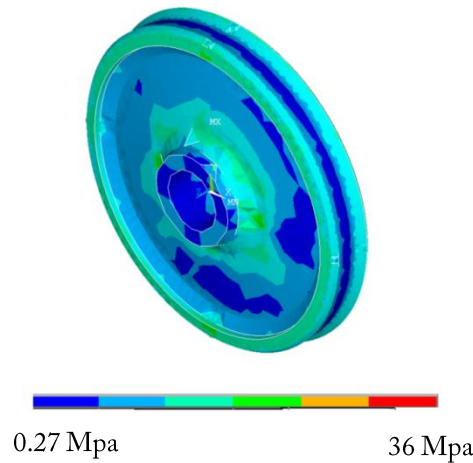
Unperforated Wheel	
Parameter	Value
$X = \dfrac{S_y}{max[(VMT)_n]}$	11.4

Figure 18. Stress situation of the unperforated wheel. Image form the Finite Element software ANSYS APDL.

5.3   Perforated wheel Results

In order to illustrate better the results obtained, a colour code is applied for each GA tuning: **red** for tuning 1, **blue** for tuning 2 and **turquoise** for tuning 3. The number of generations and population sizes increase with each tuning, but are not the same for each row-case optimization. This is mainly due to the different computational cost of each case, and due to the fact no references were found on what population size and generations are used in similar problems. Note that the other tuning values which define the GA are left default to the specifications of the GA optimizer '*ga*' in Matlab R2015b.

5.3.1 Approach 1: Directly minimizing $A_{P,3/8}$

5.3.1.1 Approach 1. 1-Row Optimization

Acoustic power curves
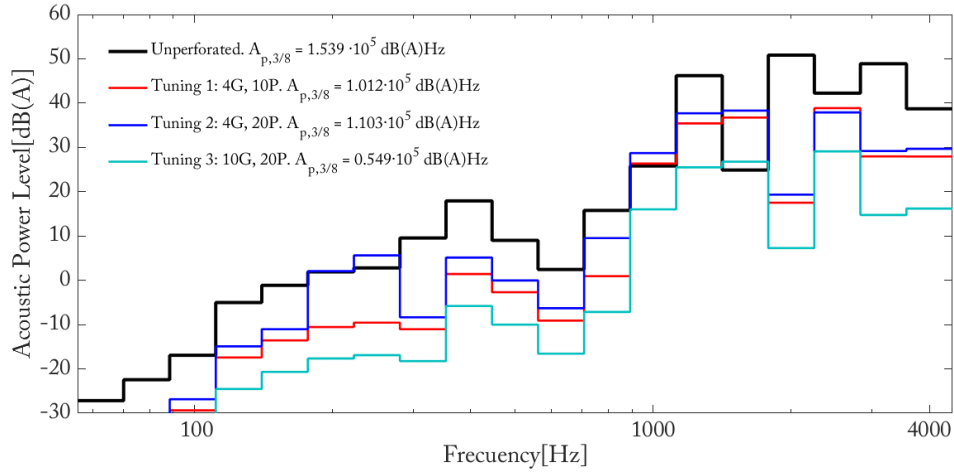
Figure 19. Power Curves and the value of Area below the curves, of the 2-row optimization loops using Approach 2, with different GA tuning parameters.

Tuning 1	
Parameter	Value
Generations	4
Population Size	10
Comp. Time [hrs]	19.6
$A_{p,3/8}$ [dB(A)Hz]	$1.012 \cdot 10^5$

Tuning 2	
Parameter	Value
Generations	4
Population Size	20
Comp. Time [hrs]	N/A
$A_{p,3/8}$ [dB(A)Hz]	$1.103 \cdot 10^5$

Tuning 3	
Parameter	Value
Generations	10
Population Size	20
Comp. Time [hrs]	64.4
$A_{p,3/8}$ [dB(A)Hz]	$0.549 \cdot 10^5$

Tables 7-9 (from left to right). Relevant data for analysis, for each different GA tuning.

Optimization data

Figure 20. Evolutive path of the maximization of mean eigenfrequencies for each tuning.

44
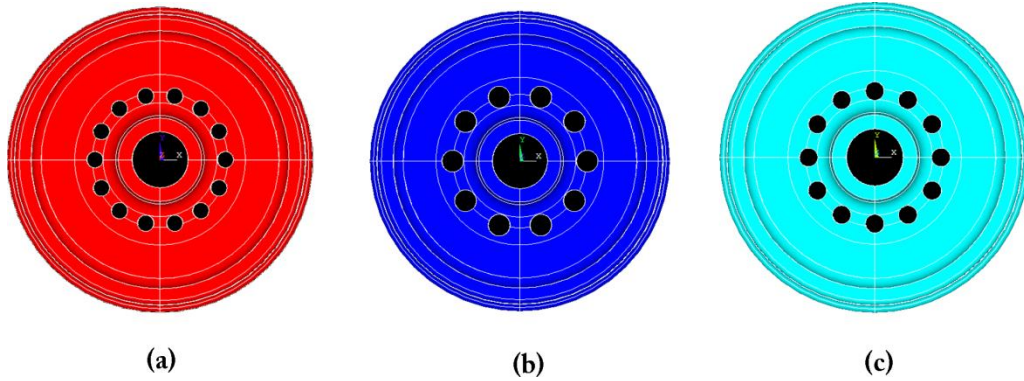
Tuning 1	
Variable	**Value**
X$_1$	0,25m
R$_1$	0,03125m
N$_1$	14

Tuning 2	
Variable	**Value**
X$_1$	0,2625m
R$_1$	0,0425m
N$_1$	10

Tuning 3	
Variable	**Value**
X$_1$	0,25m
R$_1$	0,035m
N$_1$	12

Figure 21. Wheel Optimum designs and their corresponding optimum variables found for this analysi.

Comment

In these optimization loops, similar designs (Figure 21), were found by the algorithm which shows a good agreement throughout the different GA tunings. Similar designs however, have quite different noise radiation levels (comparing Tuning 3 with Tuning 2, for example), which shows a high sensibility of the objective function with respect to the design variables.

Overall, the three settings produced good results as compared to unperforated wheels, especially Tuning 3 which decreased noise levels in almost all the frequency range. Special mention to the fact that Tuning 2 produced worst results than Tuning 1, even it had a larger population size. A possible explanation for this phenomenon is that GA is highly stochastic, and that if a large sample of tunings were tested, on average those with higher population and generations will have better results.

5.3.1.2 Approach 1. 2-Row Optimization

Acoustic power curves
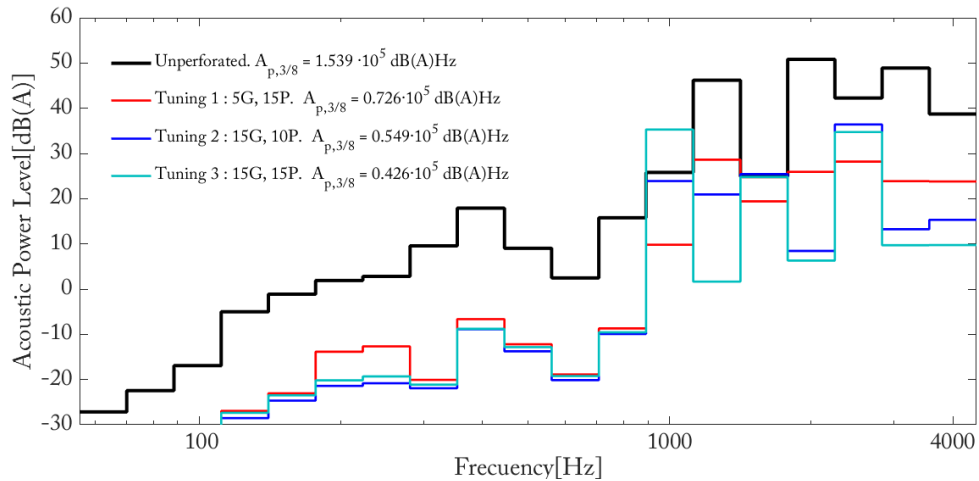
Figure 22. Evolutive path of the maximization of mean eigenfrequencies for each tuning.

Tuning 1	
Parameter	Value
Generations	5
Population Size	15
Comp. Time [hrs]	15.25h
$A_{p,3/8}$ [dB(A)Hz]	$0.726 \cdot 10^5$

Tuning 2	
Parameter	Value
Generations	10
Population Size	15
Comp. Time [hrs]	32.03h
$A_{p,3/8}$ [dB(A)Hz]	$0.549 \cdot 10^5$

Tuning 3	
Parameter	Value
Generations	15
Population Size	15
Comp. Time [hrs]	46.42h
$A_{p,3/8}$ [dB(A)Hz]	$0.426 \cdot 10^5$

Tables 10–12 (from left to right). Relevant data for analysis, for each different GA tuning.
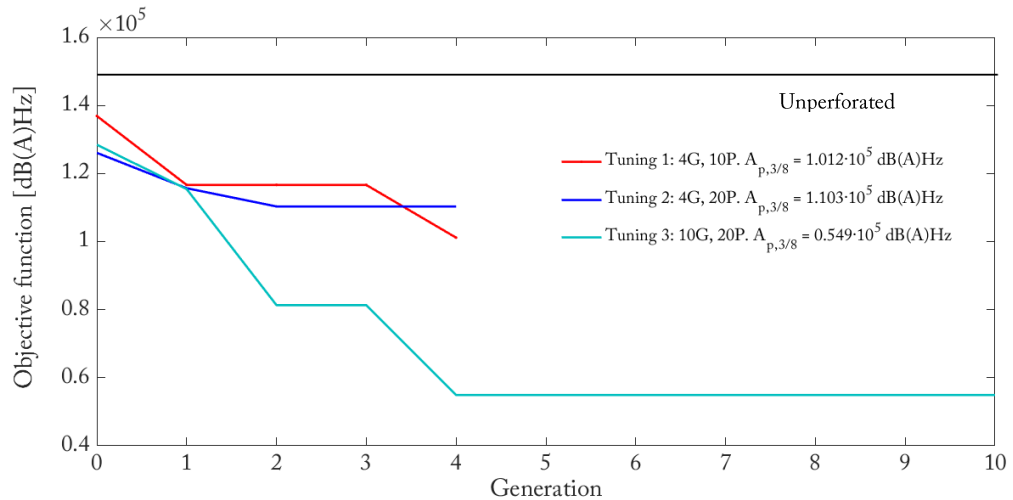
Optimization data

Figure 23. Evolutive path of the maximization of mean eigenfrequencies for each tuning. Note that Tuning 2 stopped in Generation 10 due to an unexpected informatics error.
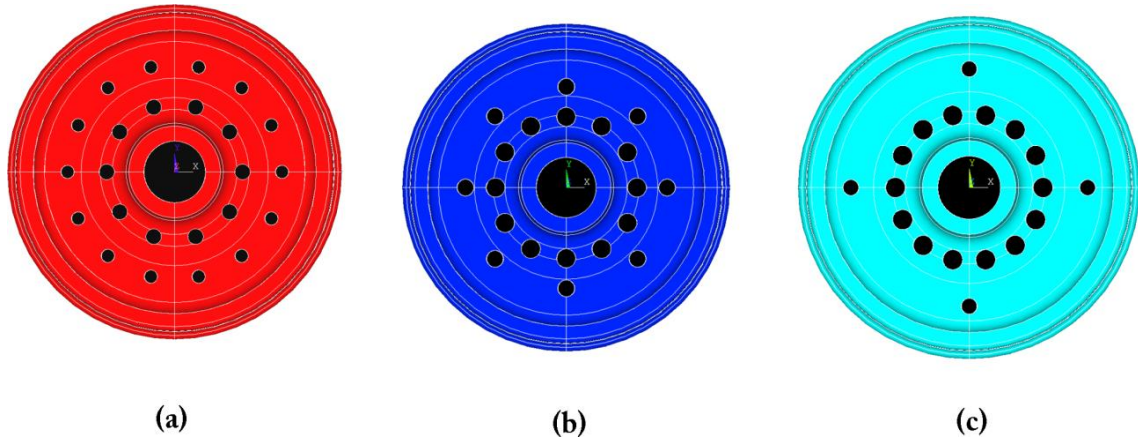
Tuning 1	
Variable	**Value**
X_1	0,2375m
R_1	0,027m
N_1	10
X_2	0,375m
R_2	0,023m
N_2	14

Tuning 2	
Variable	**Value**
X_1	0,2525m
R_1	0,034m
N_1	12
X_2	0,36m
R_2	0,03m
N_2	8

Tuning 3	
Variable	**Value**
X_1	0,2525m
R_1	0,034m
N_1	14
X_2	0,405m
R_2	0,027m
N_2	4

Figure 24. Wheel Optimum designs and their corresponding optimum variables found for this analysis.

Comment

The optimizations with 2 rows of perforations reduced considerably the acoustic emission, being the most computationally-expensive optimization (15 generations and 15 candidates per generation) the most effective optimization (Tuning 3). It is interesting to observe that Tunings 2 and 3 from this section produced similar X_1, R_1, N_1 parameters to Tuning 3 from 5.3.1 (a), 1-row optimization. This last observation explain the high fitness of this type of first-row scheme.

5.2.1.3 Approach 1. 3-Row Optimization

Acoustic power curves
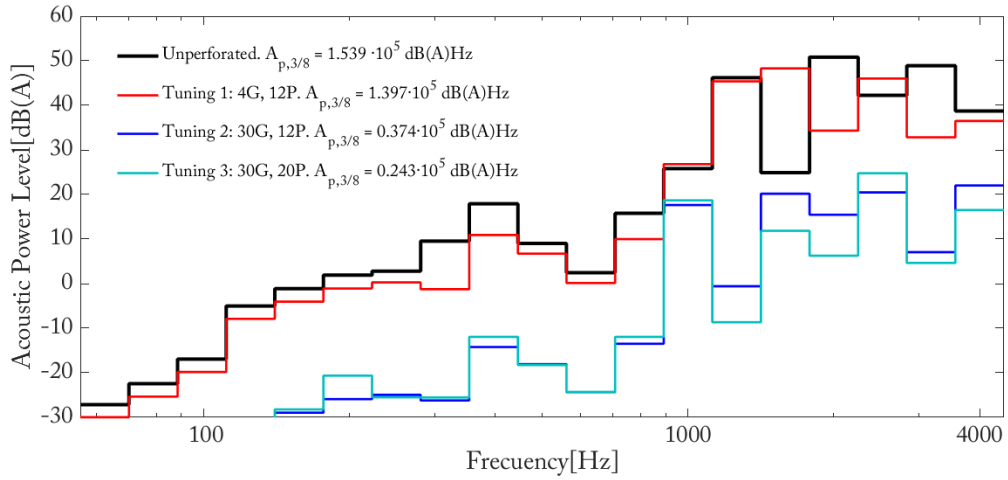
Figure 25. Evolutive path of the maximization of mean eigenfrequencies for each tuning.

Tuning 1	
Parameter	Value
Generations	4
Population Size	12
Comp. Time [hrs]	N/A
$A_{p,3/8}$ [dB(A)Hz]	$1.397 \cdot 10^5$

Tuning 2	
Parameter	Value
Generations	30
Population Size	12
Comp. Time [days]	6(aprox.)
$A_{p,3/8}$ [dB(A)Hz]	$0.374 \cdot 10^5$

Tuning 3	
Parameter	Value
Generations	30
Population Size	20
Comp. Time [days]	10(aprox.)
$A_{p,3/8}$ [dB(A)Hz]	$0.243 \cdot 10^5$

Tables 13–15 (from left to right). Relevant data for analysis, for each different GA tuning.
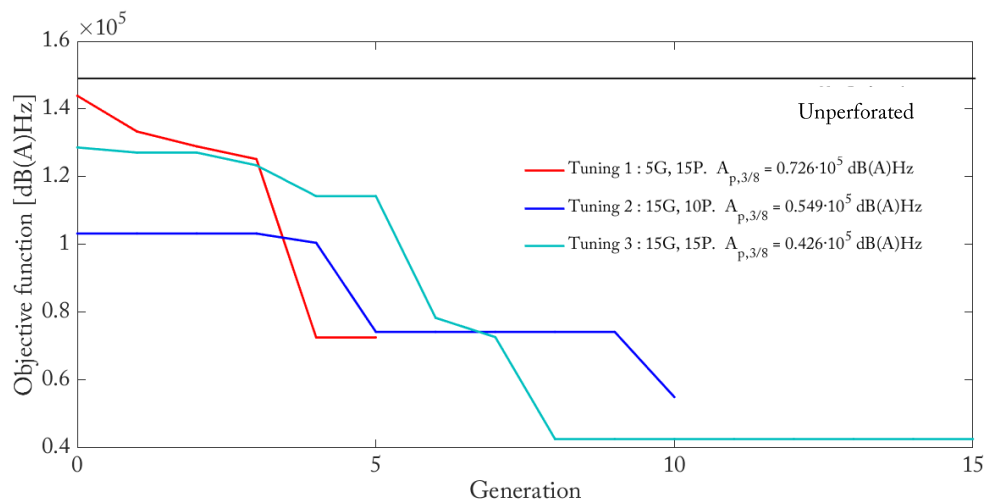
Optimization data

Figure 26. Evolutive path of the maximization of mean eigenfrequencies for each tuning.

(a)   (b)   (c)

Tuning 1	
Variable	**Value**
X_1	0,255m
R_1	0,0345m
N_1	8
X_2	0,4m
R_2	0,0343m
N_2	4
X_3	0.41
R_3	0.025
N_3	12

Tuning 2	
Variable	**Value**
X_1	0,25m
R_1	0,031m
N_1	16
X_2	0,32m
R_2	0,033m
N_2	12
X_3	0.41
R_3	0.026
N_3	10

Tuning 3	
Variable	**Value**
X_1	0,205m
R_1	0,035m
N_1	14
X_2	0,335m
R_2	0,028m
N_2	4
X_3	0.4225
R_3	0.025
N_3	4

Figure 27. Optimum designs and their corresponding optimum variables found for this analysis.

Comment

3-row optimizations drastically reduced noise emissions. In this case, Tuning 1 had only 4 generations to explore the effect this low value had on the results. We can see that it didn't 'have' enough chances to improve and stayed in a modest fitness function value. However, Tunings 2 and 3, with a higher computational cost, produced significantly low values of $A_{P,3/8}$. In the best result, Tuning 3, we can observe a certain similarity with Tuning 3 from the last section, with almost equal R_1, N_1 and N_2.

5.3.1.4 Approach 1. n-Row Optimization

Acoustic power curves
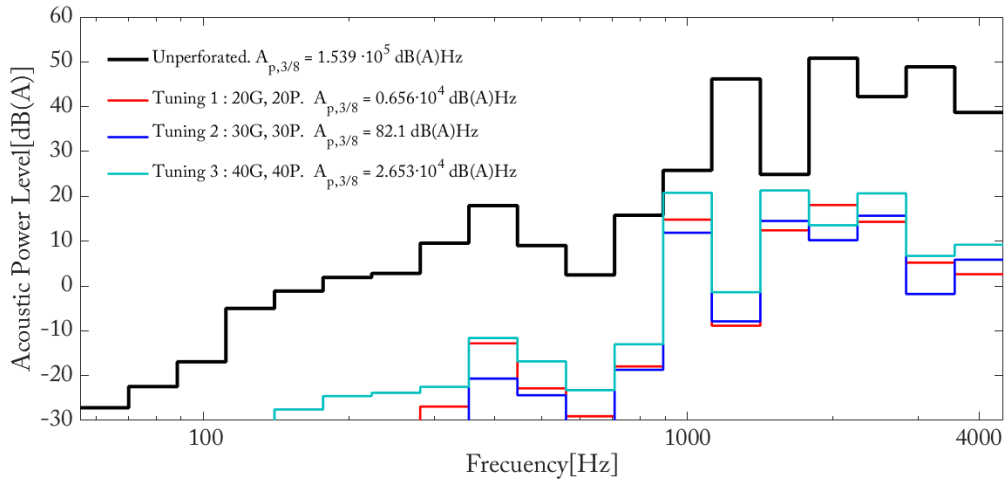
Figure 28. Evolutive path of the maximization of mean eigenfrequencies for each tuning.

Tuning 1	
Parameter	Value
Generations	20
Population Size	20
Comp. Time	N/A
$A_{p,3/8}$ [dB(A)Hz]	$0.656 \cdot 10^4$

Tuning 2	
Parameter	Value
Generations	30
Population Size	30
Comp. Time	N/A
$A_{p,3/8}$ [dB(A)Hz]	82.1

Tuning 3	
Parameter	Value
Generations	40
Population Size	40
Comp. Time]	N/A
$A_{p,3/8}$ [dB(A)Hz]	$0.265 \cdot 10^5$

Tables 16–18 (from left to right). Relevant data for analysis, for each different GA tuning.
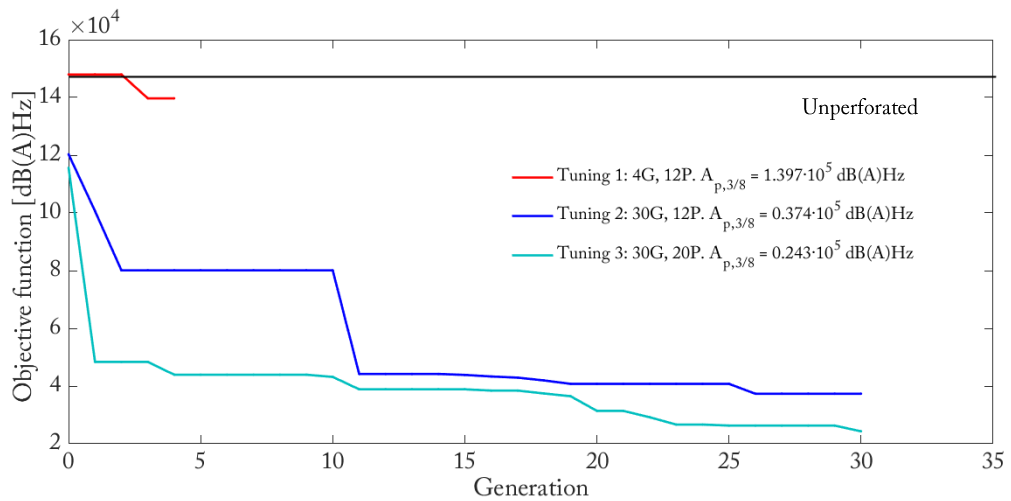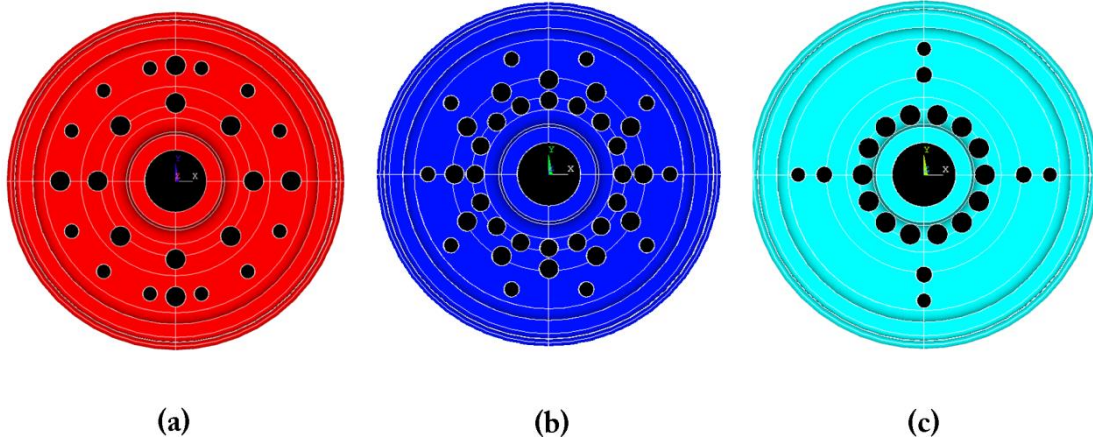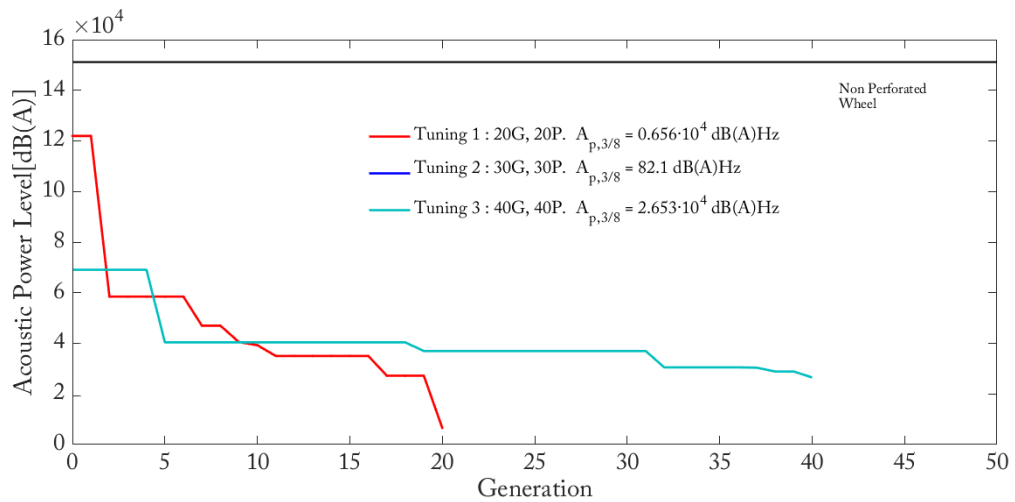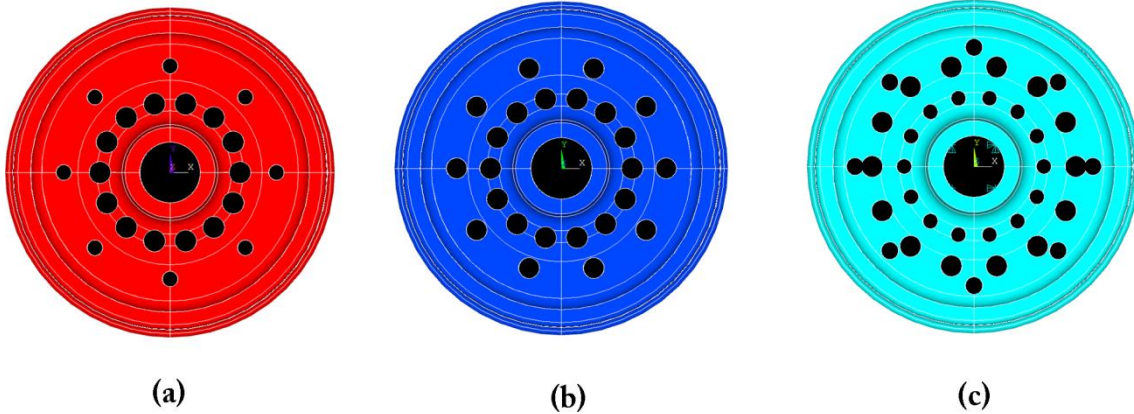
Optimization data

Figure 29. Evolutive path of the maximization of mean eigenfrequencies for each tuning. Note that Tuning 2 did not produce a GA curve due to a programming error.

A

Optimal values for this analysis

(a)   (b)   (c)

Tuning 1	
Variable	**Value**
X_1	0,2875m
R_1	0,0385m
N_1	14
X_2	0,3775m
R_2	0,0275m
N_2	8

Tuning 2	
Variable	**Value**
X_1	0,248m
R_1	0,038m
N_1	14
X_2	0,3675m
R_2	0,0365m
N_2	10

Tuning 3	
Variable	**Value**
X_1	0,245m
R_1	0,0265m
N_1	14
X_2	0,3575m
R_2	0,0376m
N_2	14
X_3	0.4175
R_3	0.0305
N_3	8

Figure 30. Optimum designs and their corresponding optimum variables found for this analysis.

Comment

The n-row optimization, where the number of rows of perforations is an additional parameter to be optimized, produced interesting results, with very low radiation levels.

In this optimization study, Tuning 2 produced the best result from all the previous studies. Its low penalty value, of just $A_{p,3/8}$= 82.1 [dBHz] is orders of magnitude lower from the unperforated wheel, and reduces the dB(A) values along the whole frequency domain analysed. Tuning 1 also produced a similar optimal scheme as Tuning 2, with very similar N_1 and R_1 values. However, its penalty value is relatively higher than Tuning 1, being however, one of the lowest analysed. 2-row schemes are superior than 3-row schemes when the optimizer has the choice of number of rows selection as one parameter more.

5.3.2   Approach 2: Maximizing mean eigenfrequencies.

5.3.2.1 Approach 2. 1-Row Optimization

Acoustic power curves
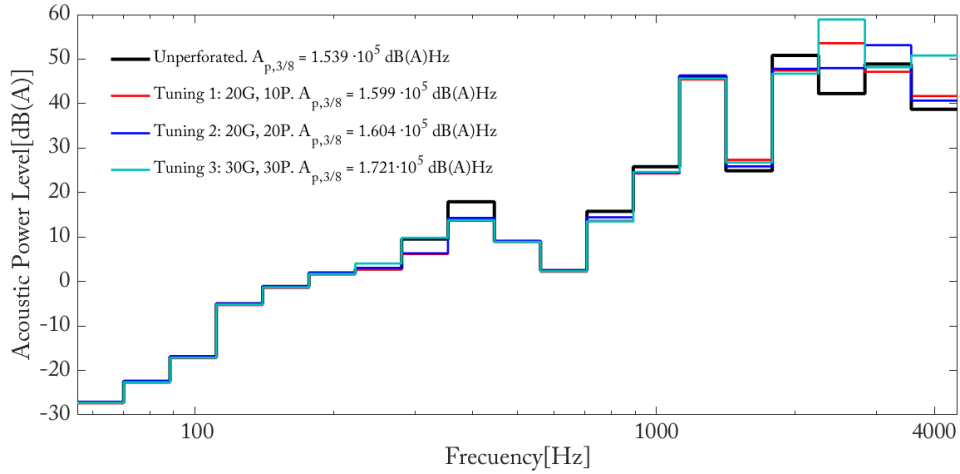
Figure 31. Power Curves and the value of Area below the curves, of the 1-row optimization loops using Approach 2, with different GA tuning parameters.

Tuning 1	
Parameter	Value
Generations	20
Population Size	10
Comp. Time [hrs]	1.5
$A_{p,3/8}$ [dB(A)Hz]	$1.599 \cdot 10^5$

Tuning 2	
Parameter	Value
Generations	20
Population Size	20
Comp. Time [hrs]	1.77
$A_{p,3/8}$ [dB(A)Hz]	$1.604 \cdot 10^5$

Tuning 3	
Parameter	Value
Generations	30
Population Size	30
Comp. Time [hrs]	5.97
$A_{p,3/8}$ [dB(A)Hz]	$1.721 \cdot 10^5$

Tables 19-21 (from left to right). Relevant data for analysis, for each different GA tuning.

Optimization data

Figure 32. Evolutive path of the maximization of mean eigenfrequencies for each tuning.

(a)   (b)   (c)

Tuning 1	
Variable	Value
X_1	0,4m
R_1	0,0319m
N_1	10

Tuning 2	
Variable	Value
X_1	0,4313m
R_1	0,0219m
N_1	10

Tuning 3	
Variable	Value
X_1	0,4m
R_1	0,03m
N_1	10

Figure 33. Wheel Optimum designs and their corresponding optimum variables found for this analysis

Comment

This optimization case has not reduced noise radiation in any of the optimization loops. The tuning with more generations and more population size (Tuning 3) has shown to be the 'noisiest' wheel, followed by Tuning 2 and Tuning 3. Surprisingly, the latter produced the best results of the three cases (however, not better than an unperforated wheel), although it was more economically tuned, with the least number generations and populations size.

This anomalous results are probably caused by the fact that, to maximize natural frequencies (which is the objective function) with one row of holes, the GA 'places' them as externally as possible, as can be seen in the three cases of Figure 33. With this pattern however, critical modes of vibration are possibly excited producing a higher acoustic power radiation, which Approach 2 cannot detect as its goal is to maximize eigenfrequencies. This can be seen comparing the results obtained in the present case with those presented in 5.3.1 (a), which are placed internally rather than externally.

5.3.2.2 Approach 2. 2-Row Optimization
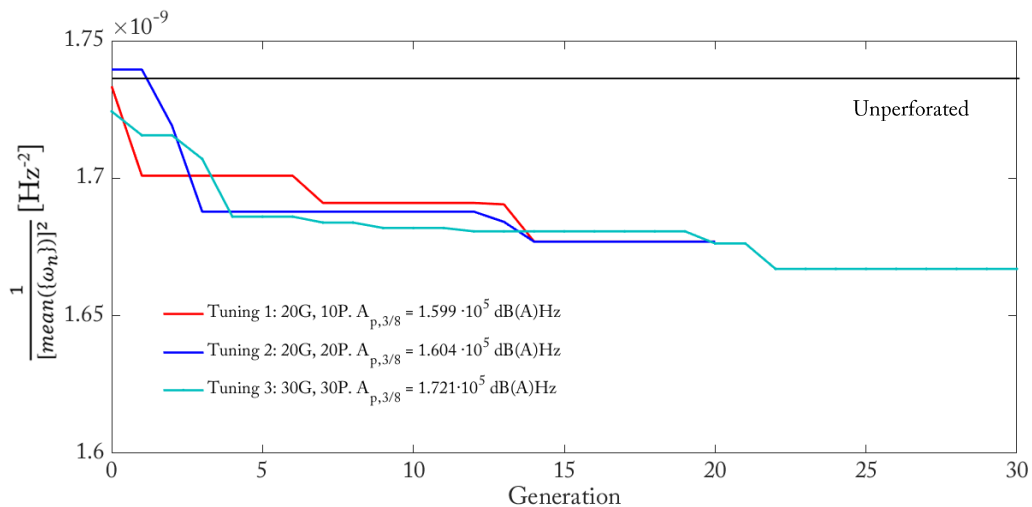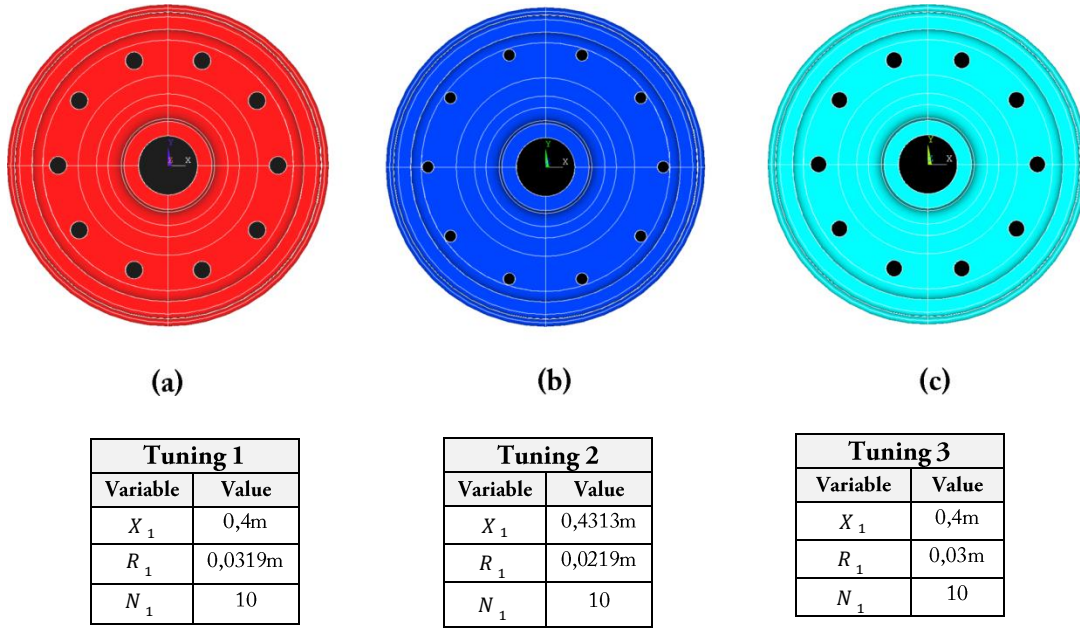
Power curves

Figure 34. Power Curves and the value of Area below the curves, of the 2-row optimization loop using Approach 2.

Tuning 1	
Parameter	Value
Generations	25
Population Size	20
Comp. time [hrs]	N/A
$A_{p,3/8}$ [dB(A)Hz]	$1.386 \cdot 10^5$

Tuning 2	
Parameter	Value
Generations	20
Population Size	30
Comp. time [hrs]	4.84
$A_{p,3/8}$ [dB(A)Hz]	$1.554 \cdot 10^5$

Tuning 3	
Parameter	Value
Generations	20
Population Size	40
Comp. time [hrs]	6.19
$A_{p,3/8}$ [dB(A)Hz]	$1.331 \cdot 10^5$

Tables 22-24 (from left to right). Relevant data for analysis, for each different GA tuning.

Optimization data

Figure 35. Evolutive path of the maximization of mean eigenfrequencies for each tuning.

(a)

(b)

(c)
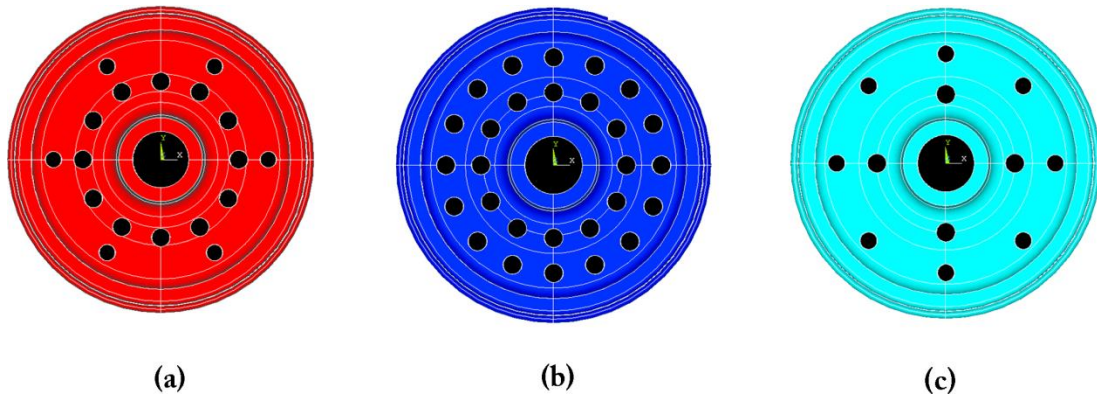
Tuning 1	
Variable	Value
X_1	0,2975m
R_1	0,035m
N_1	12
X_2	0,41m
R_2	0,031m
N_2	6

Tuning 2	
Variable	Value
X_1	0,27m
R_1	0,035m
N_1	12
X_2	0,4m
R_2	0,035m
N_2	16

Tuning 3	
Variable	Value
X_1	0,26m
R_1	0,036m
N_1	4
X_2	0,4125m
R_2	0,0325m
N_2	8

Figure 36. Wheel Optimum designs and their corresponding optimum variables found for this analysis.

Comment

Tunings 1 and 3 produced similar optimal solutions in terms of eigenfrequencies (Figure 35) and noise radiation (Figure 34). Tuning 1, which has the same generations but lower population size shows a faster convergence than Tuning 3, possibly because the GA searches in a more coarse way, making bigger steps between candidates and quickly finding the optimality characteristics. Although Tuning 1 and 3 are geometrically quite different in number of perforations, they both share similar parameters X_1, X_2, R_1 and R_2 which interestingly are very near the upper boundaries.

The GA in Tuning 2 does not converge as well as in the two other GA settings, and this is reflected when calculating its $A_{p,3/8}$ which is higher than the unperforated wheel.
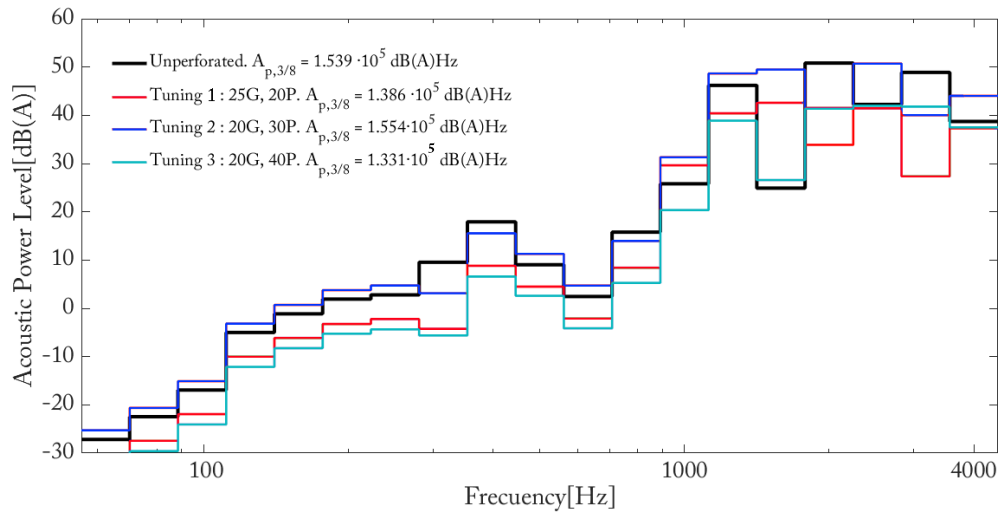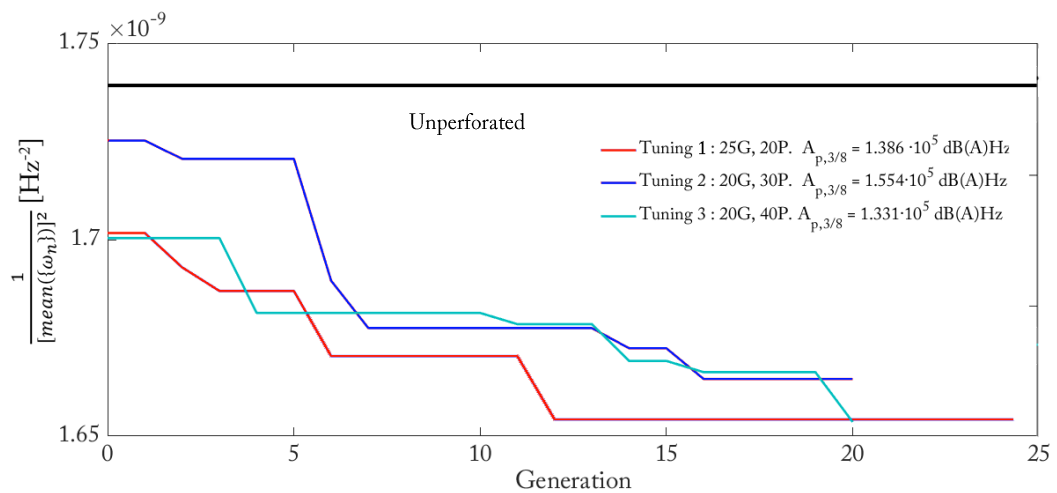
5.3.2.3 Approach 2. 3-Row Optimization
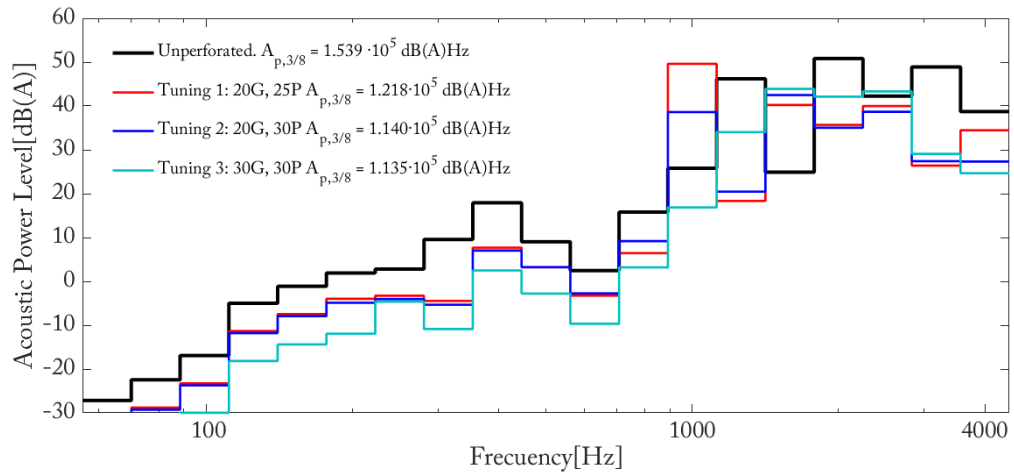
Power curves

Figure 37. Power Curves and the value of Area below the curves, of the 3-row optimization Loop using Approach

Tuning 1	
Parameter	Value
Generations	20
Population Size	25
Comp. time [hrs]	N/A
$A_{p,3/8}$ [dB(A)Hz]	$1.218 \cdot 10^5$

Tuning 2	
Parameter	Value
Generations	20
Population Size	30
Comp. time [hrs]	4.93
$A_{p,3/8}$ [dB(A)Hz]	$1.140 \cdot 10^5$

Tuning 3	
Parameter	Value
Generations	30
Population Size	30
Comp. time [hrs]	6.79
$A_{p,3/8}$ [dB(A)Hz]	$1.135 \cdot 10^5$

Tables 25-27 (from left to right). Relevant data for analysis, for each different GA tuning.

Optimization data

Figure 38. Evolutive path of the maximization of mean eigenfrequencies for each tuning.

(a)   (b)   (c)

Tuning 1	
Variable	Value
X_1	0,26m
R_1	0,033m
N_1	12
X_2	0,36m
R_2	0,031m
N_2	16
X_3	0.41
R_3	0.031
N_3	8

Tuning 2	
Variable	Value
X_1	0,26m
R_1	0,0375m
N_1	12
X_2	0,3225m
R_2	0,032m
N_2	14
X_3	0.40875
R_3	0.034
N_3	10

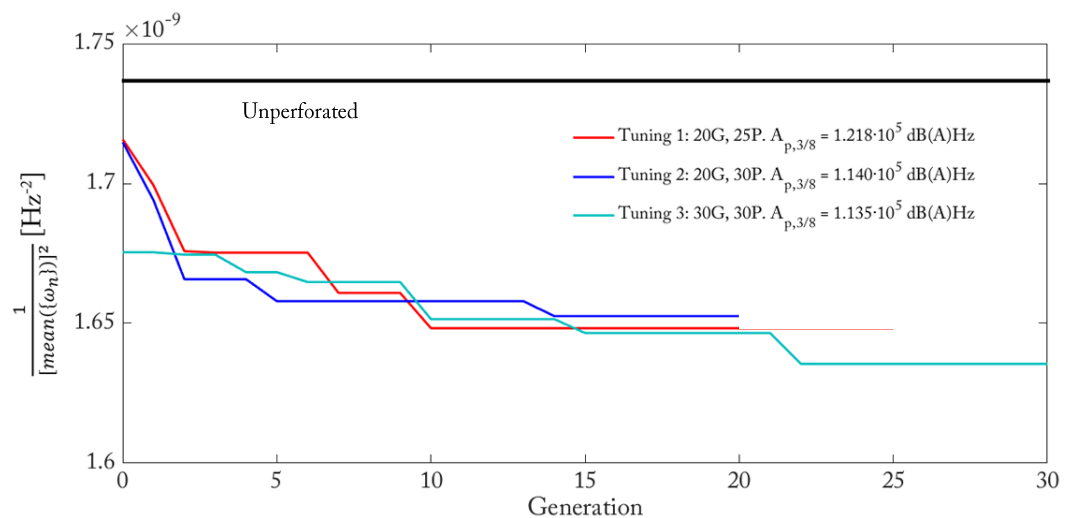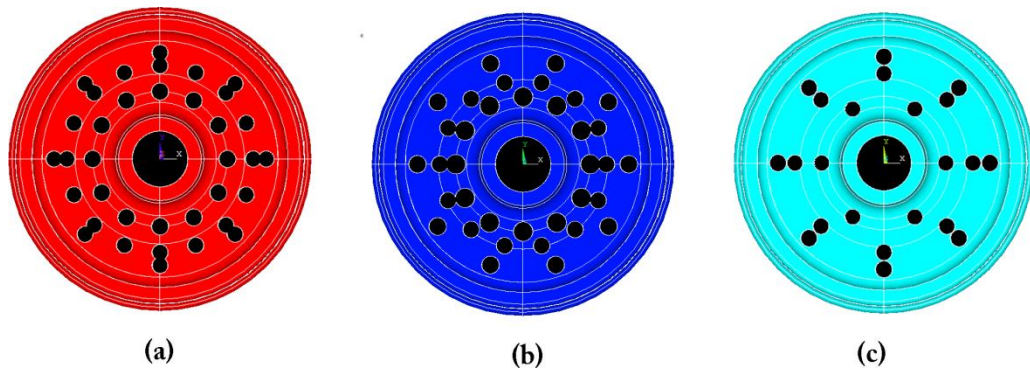| Tuning 3	
Variable	Value
X_1	0,2425m
R_1	0,0305m
N_1	6
X_2	0,3475m
R_2	0,0315m
N_2	8
X_3	0.41375
R_3	0.033
N_3	8

Figure 39. Wheel Optimum designs and their corresponding optimum variables found for this analysis

Comment

For this trial, the three optimization settings show similar GA convergence towards relatively similar eigenfrequency maximization. The three cases produce more 'silent' designs than a not-perforated wheel, being the more computationally expensive Tuning 3, the best candidate of them all. The logical relationship between population size-objective function and generations-objective function can be observed in this optimization case.

It is worth to mention that sometimes perforation schemes merge two holes creating a compound hole (seen on Tuning 2 and Tuning 1), and sometimes produce thin walls between holes (Tuning 3). These cases might be seen as structurally inviable, but the reader is reminded that all candidates passed the structural test explained in Chapter 2.

5.3.2.4 Approach 2. n-Row Optimization
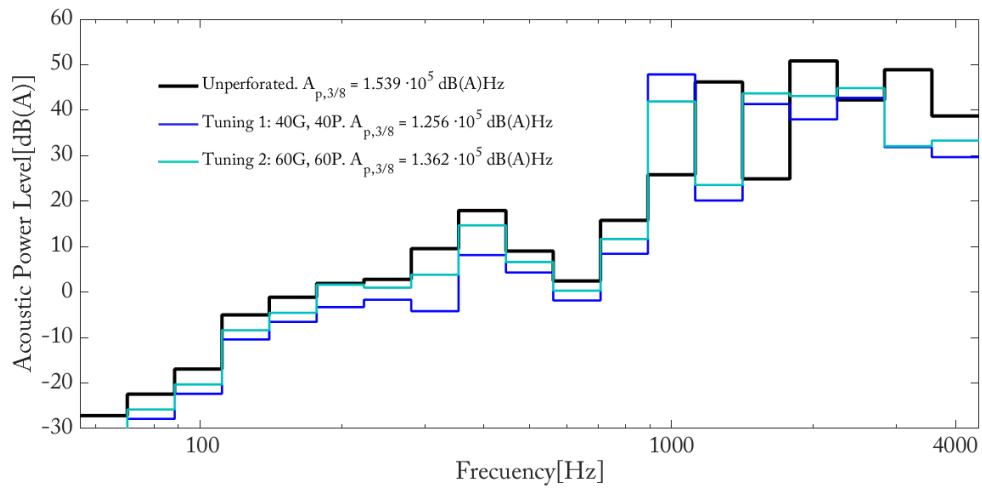
Acoustic power curves

Figure 40. Evolutive path of the maximization of mean eigenfrequencies for each tuning for the n-row optimization strategy of Approach 2 .

Tuning 1	
Parameter	Value
Generations	40
Population Size	40
Comp. Time [hrs]	N/A
$A_{p,3/8}$ [dB(A)Hz]	$1.256 \cdot 10^5$

Tuning 2	
Parameter	Value
Generations	60
Population Size	60
Comp. Time [hrs]	11.7[1]
$A_{p,3/8}$ [dB(A)Hz]	$1.362 \cdot 10^5$

Tables 28 and 29 Relevant data for analysis, for each different GA tuning.
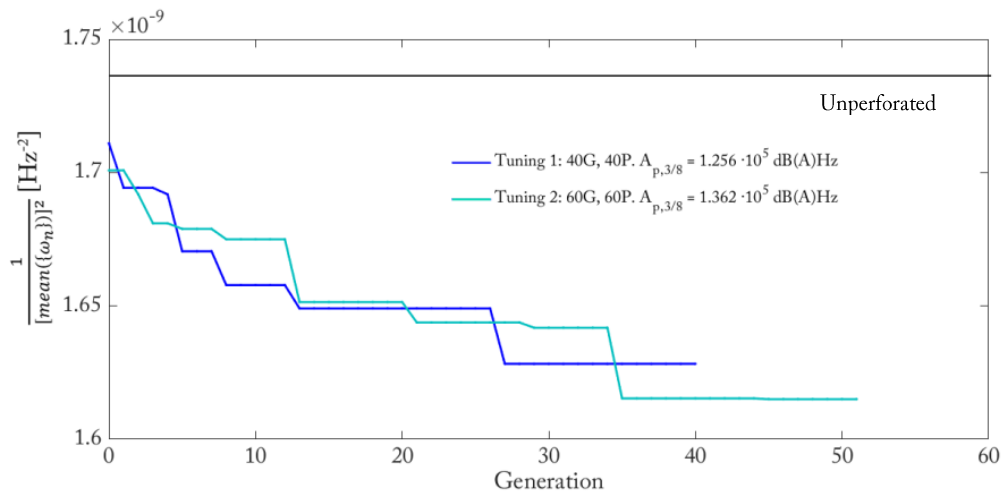
Optimization data

Figure 41. Evolutive path of the maximization of mean eigenfrequencies for each tuning.

58
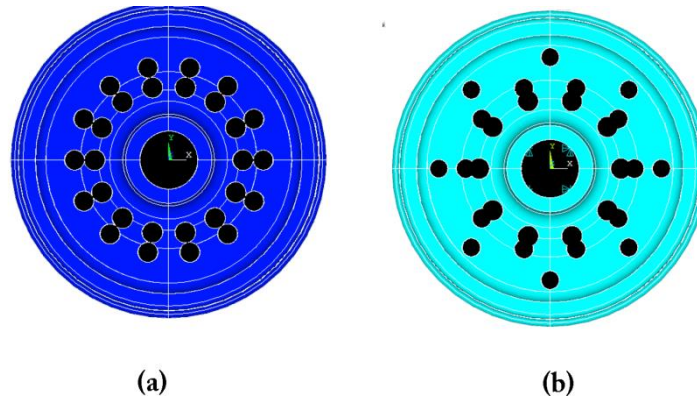
Tuning 1	
Variable	**Value**
X_1	0,275m
R_1	0,0385m
N_1	14
X_2	0,35m
R_2	0,037m
N_2	14

Tuning 2	
Variable	**Value**
X_1	0,2625m
R_1	0,0385m
N_1	10
X_2	0,3125m
R_2	0,0355m
N_2	10
X_3	0.4125
R_3	0.034
N_3	8

Figure 42. Wheel Optimum designs and their corresponding optimum variables found for this analysis.

Comment

The n-row optimizer has improved the objective function for Approach 2, compared to the other counterparts in previous sections of this approach. However, when solving its acoustic radiation, they are less effective than the other cases, showing clearly that Approach 2 can sometimes be misleading and uncertain. Only two tunings were made in this case due to computational limitations.

5.3.3 Approach optima

Approach 1

Tuning 2 from 5.3.1.4 (n-row optimizations) produced the best result from all the studied cases (Figure 43(a)). It is interesting to see that this candidate shares similar inner row values with other 2-row optima, like Tuning 1 from 5.3.1.4, or with Tuning 3 from 5.3.1.2. As a negative point, the computational cost for computing this candidate was very high compared to other Approach 1 cases and orders-of-magnitude higher than the Approach 2 cases. This particular candidate found the best agreement between an optimal inner and outer row-layout. It achieved a high reduction of 1947% in the penalty value, which is also caused by a drastic minimization of negative dB(A) values, but nevertheless produced the overall best dB(A) reduction in all the power bands, including the positive ones. Being the global optimal found, this geometry will be studied later on.

Approach 2

Differently to Approach 1, 3-row optimizations produced the most effective noise reduction in Approach 2. Tuning 3 from section 5.3.2.3 was the most effective (Figure 43 (b)). As commented before, in this approach the purpose was to maximize natural frequencies, and it is demonstrated that with this technique, some results reduced noise radiation indirectly, with a considerably low computational cost.

(a)   (b)
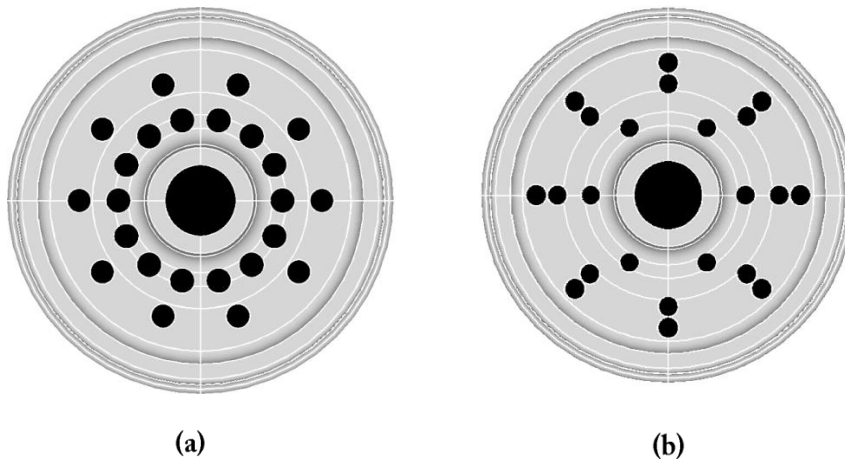
Approach 1 optimal	
Parameter	Value
$A_{p,3/8}$ [dB(A)Hz]	82.1
$A_{p,3/8}$ reduction [%]	1947%
Comp. Time [days]	>15

Approach 2 optimal	
Parameter	Value
$A_{p,3/8}$ [dB(A)Hz]	$1.135 \cdot 10^5$
$A_{p,3/8}$ reduction [%]	13.6
Comp. Time [hours]	6.72

Figure 43. Final optima for approach 1 (a) and Approach 2 (b).

5.4   Results analysis

5.4.1 Optimal perforation scheme

Reduced radiation

The most effective scheme of perforations is Tuning 2 from the optimization study in 5.3.1.4, which is repeated in Figure 44. As seen, with this geometry a reduction of the acoustic radiation has been achieved for all the studied frequency domain. In addition, the penalty value (which the GA tries to minimize) was reduced down to 0,05% its original value.
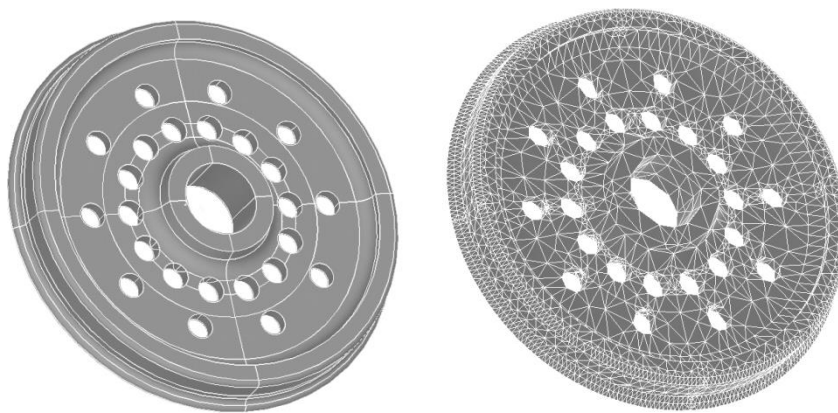
Figure 44. 3D view from the meshed optimal wheel and its mathematical representation. A relatively low discretization error can be seen.

Acoustic power curves
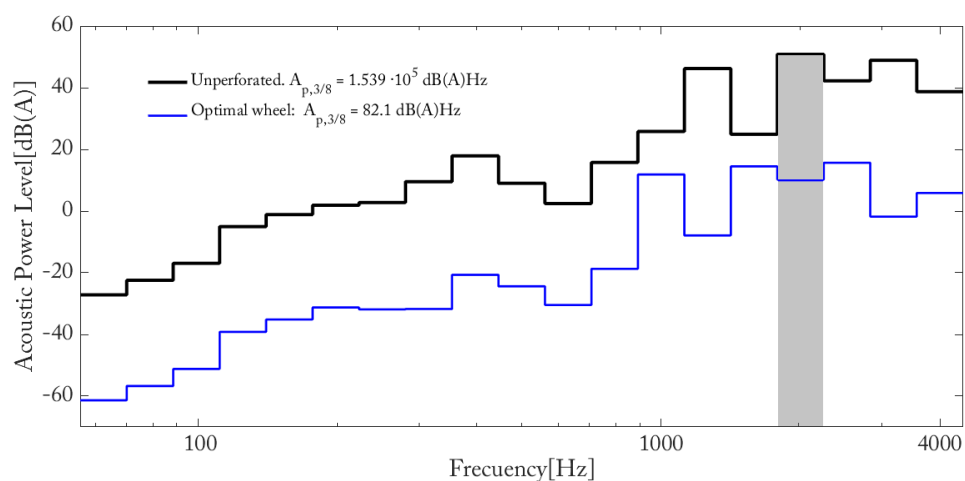
Figure 45. Radiated acoustic power for the unperforated wheel and the optimal wheel. Although levels are reduced in the whole studied domain, the very low value for $A_{p,3/8}$ is mainly caused for the drastic (yet not practical) reduction of negative dB(A) values. The shaded band corresponds to the 2106Hz mode which is later explained.

61

Being this result the one elected as the best, it is important to analyse specifically its mesh, to confirm, at least at an intuitive level, that the mathematical geometry and the discretized one do not differ importantly. In Figure 44 it can be observed how this particular candidate has an apparent low geometric discretization error, so the fatigue analysis (Figure 47) and the radiated power curves (Figure 45) are accepted.

Mode analysis.

To get a better understanding of how the optimal geometry 'achieves' less noise radiation we can analyse mode displacements of a relevant mode. In section 5.2.2 it was seen that the most radiative mode had its natural frequency at 2106 Hz. In the perforated wheel a mode with that exact frequency (Figure 46), has reduced considerably the out-of-plane (axial) displacements to 19% its original value, which is repeated in Table 30 for the reader's comfort. In fact the 'noisy' 2106 Hz mode from the unperforated wheel was seen to be displaced to 1700Hz in the perforated wheel. In general terms, we can say that in this optimal wheel the 'hazardous' modes from the unperforated wheel have been displaced to other third octave bands where they resonate lower, and thus produce less radiation.

Max. Displacement
0.0714m

Max. Displacement
0.0149m

Max. Displacement
0.0654 m
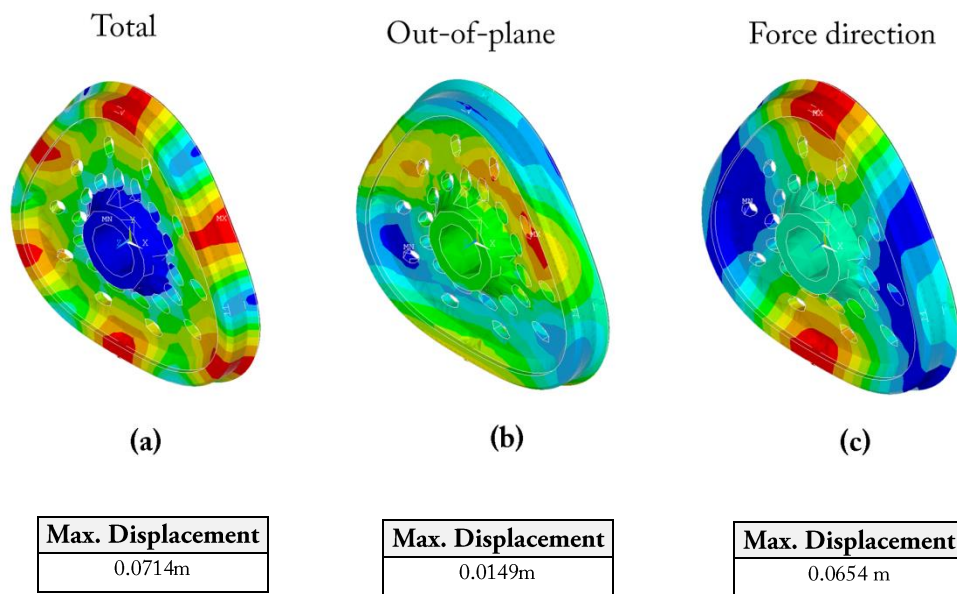
Figure 46, Modal displacements at the 2106Hz mode for the optimal wheel. (a) shows the total (sum), (b) the out-of-plane (Z axis, or axial direction) and (c) the force direction (Y-axis, or vertical direction). Note that the colour scale is relative to each result and is shown for a qualitative description. Click here to watch the corresponding animation for this mode (only for the CD format).

Maximum out-of-plane displacement of an unperforated wheel
0.079m

Table 30. Maximum axial displacements for a 2106Hz mode of an unperforated wheel.

Structural resistance

Figure 47 shows the von Misses stress plot after the fatigue analysis, validating its structural resistance with a safety factor of $X_{opt} = 4.04$ which was reduced considerably from the unperforated wheel with $X_{unp} = 11.4$, possibly as a cause of the reduced radial section and stress raisers.

1.8 Mpa   99 Mpa
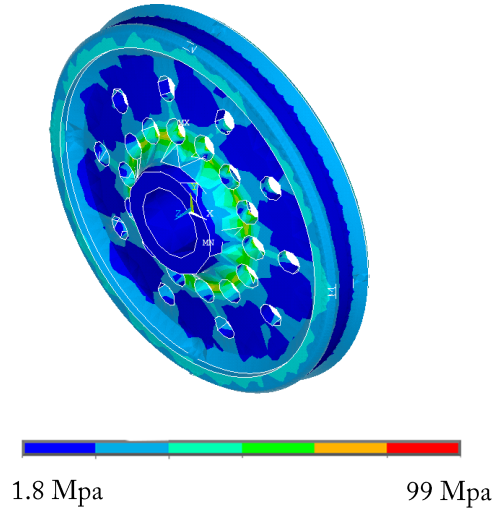
Unperforated Wheel	
Parameter	Value
$X_{opt} = \dfrac{S_y}{max[(VMT)_n]}$	4.04

Figure 47. Stress situation of the optimal perforated wheel. Image form the Finite Element software ANSYS APDL.

5.4.2 Approach comparison.

The results show that Approach 1 is more effective than Approach 2 when minimizing noise radiation. Of course, this is because Approach 1 uses a direct technique, reducing a magnitude related to the overall radiation spectrum. Approach 2 is effective when maximizing natural frequencies, however when solving its optima's power levels, it is found that noise reduction is not as effectively achieved (although it occurs to a certain extent).

As a drawback for Approach 1, its computational cost is very high. Taking a closer look at the computational expense of each task in an Approach 1 solver analysis, it can be observed that over a 98% of the computation time is spent solving the differential equation needed to calculate node velocities from the modal displacements.

Approach 2, however, avoids this process (along others, like velocity coordinate transformation, or surface data computation) as it only needs to solve the quick modal analysis for eigenfrequencies.
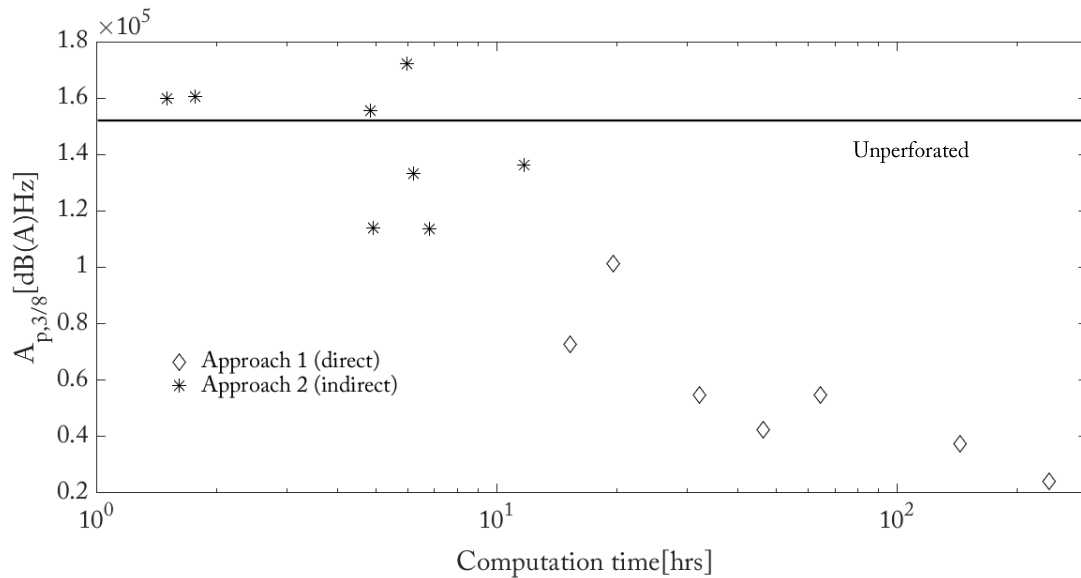
Figure 48. Some optima's objective function for both approaches and their corresponding computation time.

In Figure 48, we can observe the relationship between computational expense and the objective function for each approach. It can be seen here how Approach 2 is less expensive while not so effective, and Approach 1 produces the best results when computational resources are available. From this Figure we can intuitively notice a logarithmic relationship between the computational time and the objective function.

5.4.3 Theoretical Validation

Of course, the best way of validating the results is to manufacture them and test the response in the entire studied frequency domain. Due to the high cost of this validation method, it was not performed. Theoretical validation through commercial software is also possible. For example: the software TWINS is a potent tool for acoustics and could be used to compare the response of an unperforated wheel (wheel perforation analysis is not available in TWINS). The inconvenient of this validation method is that TWINS makes a series of assumptions (working in the time domain and linearizing, between others) which should also be applied to the model presented in this work. The latter can be a complex task and require time, so it was not done in the present work.

The theoretical validation proposed here is based on the vibration modes of section 5.2.2. In this section we can observe how the peaks of maximum acoustic radiation occur at the natural frequency of modes which are intuitively recognised as 'noisy'. For example the 'opening umbrella'-type mode occurring at an eigenfrequency of 2106 Hz, with an almost pure axial displacement, is the mode radiating the most.

As another example, the mode occurring at 1247 Hz , which is the second most radiative mode, has an almost pure displacement in the Y-axis direction, coherent behaviour given the fact that this is the force direction. Also, in this section it has been already seen how 'noisy' modes are displaced to other frequencies and how the frequencies which had high radiation power now are dominated with modes with less axial amplitude.

As another validation, according to literature [6] it is seen that web perforation decreases power levels in the lower frequency range, which is also something seen in the presented work. Almost all of the effective results show an homogenous, high power reduction at all the lower frequencies (below 1KHz) and a lower reduction in most of the higher frequency power bands.

5.4.4 Sensitivity of the acoustic response

Observing the results in 5.3.1.1 (Approach 1. 1-Row Optimization) a clear geometric similarity between the three optima can be seen, nevertheless we find a considerable difference in their radiation levels. This example shows that the acoustic response to changes in the perforation scheme can be very sensitive.

In addition, as seen in 5.3.2.1(Approach 2. 1-Row Optimization) there are some perforation designs which can increase radiation levels, so an arbitrary perforation scheme should not be used as a benchmark for web perforation effectiveness.

6 Conclusions

In this work, a review of the methodologies used and the supporting theoretical background has been explained. In addition, a wide results spectrum has been presented and discussed in-depth for future discussion and reference. The results have been theoretically validated through the reduction of the acoustically-relevant modal displacements of the optimal wheels with respect to the unperforated starting point. Additionally, a complex acoustics optimization loop has been programmed, which can be used and improved for future projects.

The results show that an optimized scheme of perforations on the web of a railway wheel can reduce significantly the sound power level in the entire studied frequency domain. Up to a 1947 % of reduction in the area below the frequency-domain acoustic power curve, $A_{p,3/8}$, was obtained by using a more computationally-expensive direct minimization technique (Approach 1). With a computationally-lighter, indirect minimization technique (Approach 2), up to a 13.6% of reduction was achieved.

The acoustic radiation response is found to be highly sensitive to the design of a perforation pattern. Additionally, it has been observed that perforation is not always an effective technique to minimize noise radiation, as an arbitrary perforation scheme can produce higher acoustic levels than its unperforated counterpart, therefore optimization is required.

7 Future improvements

7.1 Improving the actual methodology

This section proposes some improvements for the actual method, in order to improve not only its effectiveness, but also its robustness and replicability.

7.1.1 Mesher

Mesh discretization is a crucial aspect to improve. In the actual work, refined models were avoided due to high computational cost. In further improvements of the method, it is required to improve mesh refinement or the meshing method, as it has been seen that the acoustic response is highly sensitive to the geometry. In Figure 49 we can observe how different a mathematical geometric definition of a wheel can be as compared to its discretized version (which is the actual analysed model). Curved contours are converted into angled corners, and this slight change in geometry can derive in big changes in the acoustic response, as it can be deduced observing some of the results obtained.
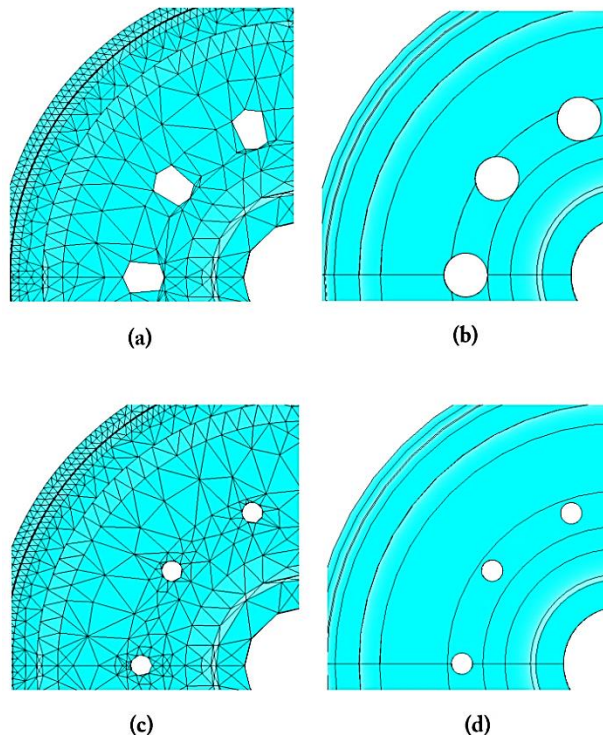
Figure 49. Details from some arbitrary designs showing the large geometric discretization error in meshed model (a) as compared to its mathematical description (b), and a lower discretization error in (c) as compared to its mathematical description (d).

7.1.2 Optimizer

The present work describes the methodology for an optimization towards noise radiation minimization but it proves an effective solution in one given type of railway wheel. It can be argued that as railway wheels do not differ relatively much in shape from the one analysed, the present work is also valid for other wheels. Although this statement is possibly correct, a main future improvement is to prove that the methodology is valid for other types of railway wheels under the same type of analysis.

In relation with parametrization, upper and lower limits as well as discretization are also important as they define the freedom of the GA search. Parameter discretization was left constant in this work. A high discretization value will permit a more precise search but reaching optimal results will be more expensive, while a low discretization will possibly skip the best solutions but converge quickly. Given the supposed high sensitivity of the problem at hand, a high discretization (along with an adequate mesh refinement) is possibly needed to achieve better results. This will depend also of the manufacturing tolerances.

In relation to Approach 2, the optimizer was set to maximize natural frequencies by 'allocating' them in the 5KHz to 7KHz range. The 7KHz upper limit, until which the modal solver extracts modes, was not set higher due to the computational expense of solving a very high number of modes. However, if the 7KHz upper limit was increased, the optimizer will have an additional margin to distribute the mode eigenfrequencies. For this improvement, a superior computational unit is possibly required.

In this optimization research, only the GA parameters Population Size and Generations have been explored. However, there are still many different GA parameters which could be modified in order to obtain better optima, like Mutation Rate, Crossover, Elitism, and many others.

7.1.3 Solver

In addition, another very relevant future work is to implement a more precise noise radiation solver, through the calculation of radiation efficiencies. Radiation efficiencies here where approximated as 1, while they can be larger (resulting in an underestimated analysis), or lower (resulting in an overestimated analysis). Nevertheless, according to the predictions in [3], web perforations decrease the radiation efficiency, potentially resulting in an even greater noise radiation reduction.

In relation to the fatigue analysis explained in 2.3, a more rigorous approach will be to create a series of analysis rotating a known Hertzian pressure distribution in a series of discrete points, which will be separated by the fraction of degrees corresponding to the nominal width of the pressure distribution. This final approach will be more accurate, but will be more computationally expensive as tenths of analyses should be made for each design candidate.

The objective function is also an important issue to improve. The fact that the penalty value, $A_{p,3/8}$ decreases for a minimization below 0dB(A) (which is the human hearing threshold) limits the effectiveness of the optimization loop. Although it is true that for most effective optima, lower $A_{p,3/8}$ values corresponded to lower power levels in almost all the studied frequency domain, an objective function which focused on minimizing positive dB(A) values instead of decreasing negative ones is desired. A possible new penalty value to minimize is written in Equation 22. Equation 22 will solve the problem of minimizing negative values, while considering information of the actual negative power area for the optimizer. Additionally, the use of the threshold value from where sound is considered noise can possibly increase the effectiveness of the optimization loop.

$$p' = \left(A_{p,3/8} - threshold \right)^2 \tag{22}$$

Where p' is the corrected penalty value and $threshold$ is the minimum dB(A) value for sound annoyance.

Finally, a very important improvement is to perform code optimization to reduce the computational cost of solving the wheel dynamics, in order to carry on the more effective Approach 1 optimizations.

7.2   Exploring other optimization techniques

Apart from a 'perforation approach', there are other types of shape optimizations which can be made in order to minimize acoustic power levels, like ones introduced in Section 2.1.2. It is however rather more interesting to introduce an area which the present literature have not yet explored for rolling noise acoustic minimization. The use of more sophisticated computational tools for optimization can lead to more surprising results, like with the use of Topology Optimization. Instead of a reduced number of shape parameters to optimize, generally Topology Optimization optimizes the material density of a selected design domain, resulting in a more extense, precise and fundamental exploration of the design space, which can derive in a radically new approach towards noise minimization.

References

[1] U.Clausen et al. : Reducing railway noise pollution. European Paliament. Directorate general for internal policies.(2012) .

[2] A.Pieringer.: On the modelling of wheel/rail noise. AIA-DAGA 2013 Merano. (2013).

[3] D.Thompson. Railway Noise and Vibration Mechanisms, Modelling and Means of Control. ISBN: 978-0-08-045147-3. (2010).

[4] D. Thompson et al. Brake and wheel design can cut train noise. Railway Gazette. (2003). Link: http://www.railwaygazette.com/news/single-view/view/brake-and-wheel-design-can-cut-train-noise.html (available in 28/03/2017)

[5] X.Tong et al. Influence of web plate holes on the radiation noise characteristics of wheels of the high speed train. Journal of Vibroengineering . Nov2016, Vol. 18 Issue 7, p4870-4884. (2016)

[6] B. Hemsworth et al. "Silent Freight and Silent Track projects", Proceedings of Internoise 2000, Nice, France. (2000).

[7] J.Cagnol et al.: Shape optimization and optimal design. Proceedings of the IFIP Conference. (2001).

[8] J.Sokolowsky et al.: Introduction to Shape Optimization. Shape Sensitivity Analysis. Springer Series in Computational Mathematics. (1992).

[9] Ashok D. : Belegund et al. Optimization Concepts and applications in Engineering Prentice Hall. ISBN 0-13-031279-7. (2003).

[10] GA. Efthimeros et al.: Vibration/noise optimization of a FEM railway wheel model. Engineering Computations, Vol. 19 Iss 8 pp. 922 – 931. (2002).

[11] J.C.O Nielsen et al.: Multi-disciplinary optimization of railway wheels. Journal of Sound and Vibration 293 510–521. (2006).

[12] E. Zitzler.: Evolutionary Algorithms for Multiobjective Optimization: Methods and Applications TIK-SCHRIFTENREIHE NR. 30. (1999).

[13] IEC 61672-1:2013 Electroacoustics - Sound level meters - Part 1: Specifications. IEC. 2013.

[14] S.L.Grasse. Rail irregularities, corrugation and acoustic roughness: characteristics, significance and effects of reprofiling. J Rail and Rapid Transit 226(5) 542–557 ! IMechE. (2012).

[15] D. Thompson et al. Experimental validation of the TWINS prediction program, Part 2: results. Journal of Sound and Vibration, 193, 137–147. (1996).

[16] D.Thompson. Theoretical modelling of wheel-rail noise generation. Proceedings of the Institutionof Mechanical Engineers. Journal of Rail and Rapid Transit, 205F, 137–149. (1991).

[17] P.E. Gautier et al "Railway wheel optimization", Proceedings of Inter Noise 93. pp. 1455-1458. (1993)

[18] P. Bouvet et al. Rolling noise from freight railway traffic: reduction of wheel radiation by means of tuned absorbers. Proceedings of Internoise 2000. (2000).

[19] D. Thompson. But are the trains getting any quieter? ICSV14 Cairns • Australia 9-12 July. (2007).

[20] C.Jones et al. Design of a railway wheel with acoustically improved cross-section and constrained layer damping. Proceedings of Internoise 2000, Nice, France, 673-678. (2000).

[21] Zhu, J. Aerodynamic noise of high-speed train bogies University of Southampton, Engineering and the Environment, Doctoral Work, 228pp. (2015).

[22] DP Connolly et al. The growth of railway ground vibration problems - A review. US National Library of Medicine National Institutes of Health. doi: 10.1016/j.scitotenv. October. (2015).

[23] Sneddon, I. N. The Relation between Load and Penetration in the Axisymmetric Boussinesq Problem for a Punch of Arbitrary Profile. Int. J. Eng. Sci. v. 3, pp. 47–57. (1965).

[24] Acoustics. Railway applications. Measurement of noise emmited by railbound vehicles. (ISO3095:2013).(2014).

[25] H. Estrada et al. Acoustic radiation efficiency of a periodically corrugated rigid piston : Appl. Phys. Lett. 101, 104103 (2012); doi: 10.1063/1.4748868 (2012).

[26] B.Thomas. Evolutionary Algorithms in Theory and Practice: Evolution Strategies, Evolutionary Programming, Genetic Algorithms. (1996).

Annex I: Articles and Conditions

I.1 Introduction

I.1.1 Scope

The objective of this document is to define the technical, facultative, legal and economic conditions that come along the acquisition of the minimization project 'Acoustic radiation minimization of railway wheels by using advanced optimization techniques', in order to specify to the client and creator their respective rights and duties. This document pretends to assure the correct interpretation of the present engineering work.

Although the present work is a Mechanical Engineering Final Degree Project, in order to write this document and the Budget document, it is supposed that the project is created by a supposed freelance engineering consulting for a client.

I.1.2 Project Briefing

The client requires the following:

- A wheel that **theoretically** minimizes in at least 20%, the area below the dB(A) acoustic radiation spectrum in the frequency domain, discretized in third octaves, with respect to a standard wheel and with a threshold intensity of $1 \cdot 10^{-12}\,\text{W/m}^2$.
- The re-designed wheel must base it shape on an existing wheel. Only post-manufacturing modifications should be made on the wheel, (such as subtracting or adding material).
- The shape modifications should be viable, both economically and technically. This means that re-manufacturing processes should be coherent with the present standard technologies and that the re-designed wheel should be structurally resistant to the design loads (which are specified later).
- The engineer in charge (creator of the project) must specify the procedures and model assumptions for the analyses developed, as well as detail the results obtained and how to manufacture them correctly.

I.2. Conditions

I.2.1 Technical Conditions

The objective of this document is to define the technical, facultative, legal and economic conditions that come along the acquisition of the minimization project 'Acoustic radiation minimization of railway wheels by using advanced optimization techniques'.

I.2.1.1 Results assessment

As explained in the Memoir document (Section 3.3), a series of mathematical assumptions in the analysis model were made, mainly, approximating the radiation efficiencies to a constant value, and the assumptions due to the Finite Element discretization.

For these reasons the creator is not responsible for any difference in the real (measured) results of a correctly manufactured perforation scheme result.

The client is referred to chapters 1-7 to technically asses how rigorous the methods developed are, since they are comprehensively explained.

I.2.1.2 Results assessment

If the client wishes to manufacture any of the results obtained (including the best optimal), then the exact perforation scheme defined in the document 'Technical drawings' must be executed.

The tolerance admitted is ±0,5mm.

- The perforation diameters do not correspond to any standard magnitude, therefore the client must manufacture the right tools to manufacture such diameters.
- The usual methods to prevent unexpected structural failure should be applied, such as edge smoothening of the already made perforations.

I.2.2. Economic Conditions

I.2.2.1 Economic Rights

- The client will be able to manufacture freely any of the results obtained and benefit economically from the success related to the physical improvement.

I.2.2.2 Economic Duties

- The client will pay the amount specified in Section 2.6 of the document 'Project Budget' of this project.
- The client will not benefit economically from reproducing the methodologies described to find new optimal designs.

I.2.3. Contract Conditions

I.2.3.1 Usage Rights

- The client will never publish the methods used to achieve the results, or will not share them with third parties. This information will only be used for the technical approval of the results obtained.

I.3 Regulations

Excepting the ones described below, there are no more regulations to be applied to this project, as it is a design optimization and no manufacturing details are considered. The client may apply all the pertinent regulations if he/she wishes to manufacture any of the results obtained.

I.3.1 Acoustics

The mathematical description of the dB(A) filter was applied according to the IEC 616272.1:2013 standard.

I.3.2 Contact Force

The dynamic force record was obtained using the pseudorandom rail roughness specified in ISO3095:2013. [24]

I.3.3 Wheel and rail material

The simulations were done with a railway wheel material which follows the UIC 812-3 R6 T,E standard and a rail material following the UIC860-0 standard. Both materials should have , at least, the properties specified in Table 2 of section 2.3.2 of Chapter 2.

I.4 Patent search

I.4.1 Similar Patents

After an extended search at the European Patent Office (EPO) libraries, no national or international patents were found regarding perforations in the web of a railway wheel for means of acoustic minimization.

As described in Chapter 2, there are various authors which have researched on the idea of noise reduction of railway wheels through wheel perforation, however as far as it concerns, no author has successfully minimized noise through an optimized design of a perforation scheme.

Annex II: Budget

II.1. Introduction

The scope of this document is to specify a budget for the optimization method developed. Its objective is to document the cost of developing such project as a way of defining the required economic price to be charged from the entity selling the project to the potential purchaser of the engineering project.

Being the product a theoretically optimal railway wheel, the costs are mainly those related to the development of it. They include the cost of using electronic hardware, software licenses required for the specific development of the project, workspace facilities (a physical office to work, water and electric supply) and engineering manpower, between others.

As the present project was developed in the city of Valencia, Spain, the reference prices are according to a business set in this location.

II.2. Budget Specifications

II.2.1 Software Licenses

Software licenses are crucial for the development of the project, as they provide the right tools and computation modules for structural analyses, programming and editing. ANSYS, Matlab and Microsoft Office were the main computer programs used.

In the table below, the costs related to license are specified. For this, we suppose that these licenses do not have a time limitation, and they can be used for other future projects of the supposed consulting enterprise. According to this, we set a 5% of estimated use of the license, accounting for at least 20 future projects with those same licenses.

Software licenses costs (all monetary values in € w/o VAT)						
Name	Description	Units	Quantity	Estimated use	Unit cost	Partial cost
Anys	Structural	Licenses	1	5%	17000	850
Matlab	R0125b academic license	Licences	1	5%	2000	100
Microsoft Office	Profesional license 2016	Licenses	1	5%	539	26,95

Licenses subtotal	976,95

Price References (as for the 6th of June 2017):

- ANSYS: Estimated
-Matlab: https://es.mathworks.com/pricing-licensing.html?prodcode=ML&intendeduse=comm
-Microsoft Office: https://products.office.com/es-es/buy/office

II.2.2 I.T Hardware

Information Technologies (I.T) equipment was used to run the required software. Due to the relatively large computational expense of the present projects, two server computation units were used for computation, as well as a central control laptop used for programming and editing tasks. In addition some other auxiliary material specified in the table below was used. The 'Estimated use' value is applied similarly as in 2.1.

I.T hardware (all monetary values in € without VAT)						
Name	Description	Units	Quantity	Estimated use	Unit cost	Partial cost
Computing unit	CPU: Intel® Xeon® es 430 @ 2.66GHz dual core RAM: 32gb OS: Windows server 2012 r2.	Units	2	5%	2400	240
Monitor	Benq gw2470h, va, full hd, 23.8"	Units	1	5%	130	6,5
Laptop	Asus f541ua-gq630t, i7-7500u, 8 gb ram, 1 tb hdd	Units	1	5%	610	30,5
Computer mouse	Logitech g203 prodigy	Units	1	5%	36	1,8
Keybord	Cherry keyboard kw2000 black-wrls	Units	1	5%	19	0,95

Hardware subtotal	279,75

Price References (as for the 6th of June 2017):

- Computing Unit: Estimated as no longer in sale.

-Monitor, laptop, computing mouse, keyboard: https://tiendas.mediamarkt.es

II.2.3 Human Labour

Given the high degree of intellectual work, such as experimental planning, programming and editing, human labour cost had the biggest share in this project. In this particular case a mechanical engineer is required for these tasks, and this person is also the freelance owner of the theoretical consulting business. For this reason, the human labour costs, minus a certain part to be deducted for taxations, will be the personal share of this project.

In the table below, the unit cost of 43,3 €/hr is obtained applying an extra 60% to a 26 €/hr net benefit. The 40% accounts for taxes like national insurance and the freelance tax ('tasa de autónomo' in Spain).

Human labour (all monetary values in €)						
Name	Description	Units	Quantity	Estimated use	Unit cost	Partial price
Mechanical engineer	Research & development	Hours	300	100%	43,3 €/hr	12990

Human resources subtotal	12990

II.2.4 Indirect Costs

These costs include the rent, supplies, transports, phone calls. They are estimated as a 5 % of the sum of subtotals from 2.1 to 2.3.

	Indirect costs (all monetary values in €)					

Name	Description	Units	Quantity	Estimated use	Unit price	Partial price
Indirect costs	Electricity, water, telephones, fungible, transport…	N/A	N/A	N/A	N/A	712,34

Supplies subtotal	712,34

Price References (as for the 6th of June 2017):

- Electricity: Red Electrica De España

-Water: OCU.org

-Internet: ONO

II.2.5 Total Costs and Market Price.

The Industrial cost is obtain adding subtotals from 2.1 to 2.4. To the industrial cost, a commercial margin of 300% is applied due to the type of project developed, this value is the net benefits for the theoretical consulting company. If the client was to be a train manufacturer they can potentially benefit from the project, collecting hundredths of thousand euros, for that reason a margin of 300% is applied. The total cost is obtained adding the commercial and industrial cost, and finally to obtain the market price a Spanish IVA is applied to the total cost. This market price is the final amount which the client will have to pay for the project.
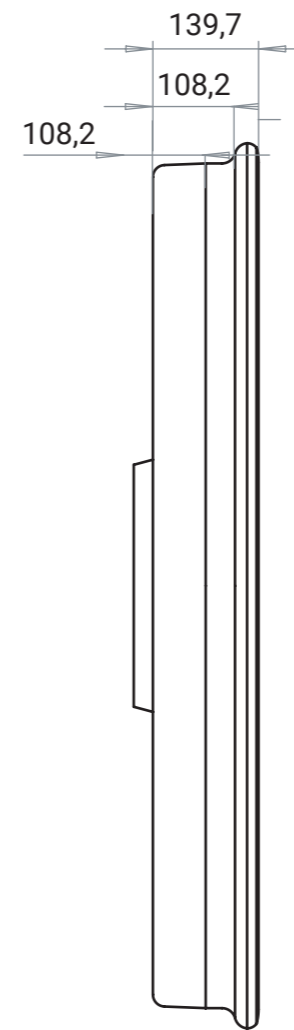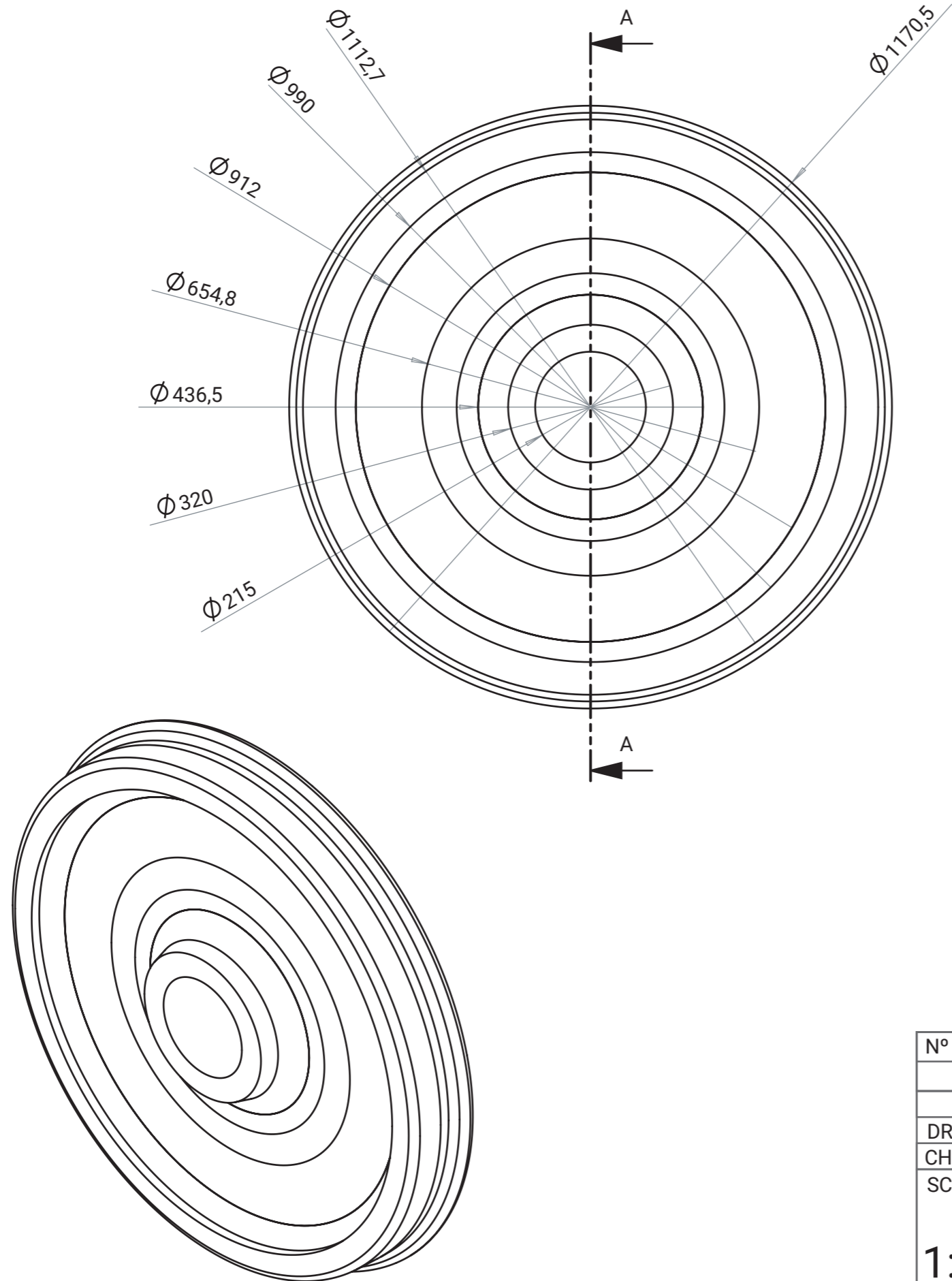
Total costs (all monetary values in €)		
Industrial cost		14959,04
Commercial margin	300%	44877,11
Total cost		59836,14
Vat	21%	12565,59

Market price	72401,73

Annex III: Technical Drawings

Ø 1112,7
Ø 990
Ø 912
Ø 654,8
Ø 436,5
Ø 320
Ø 215
Ø 1170,5

A
A

139,7
108,2
108,2
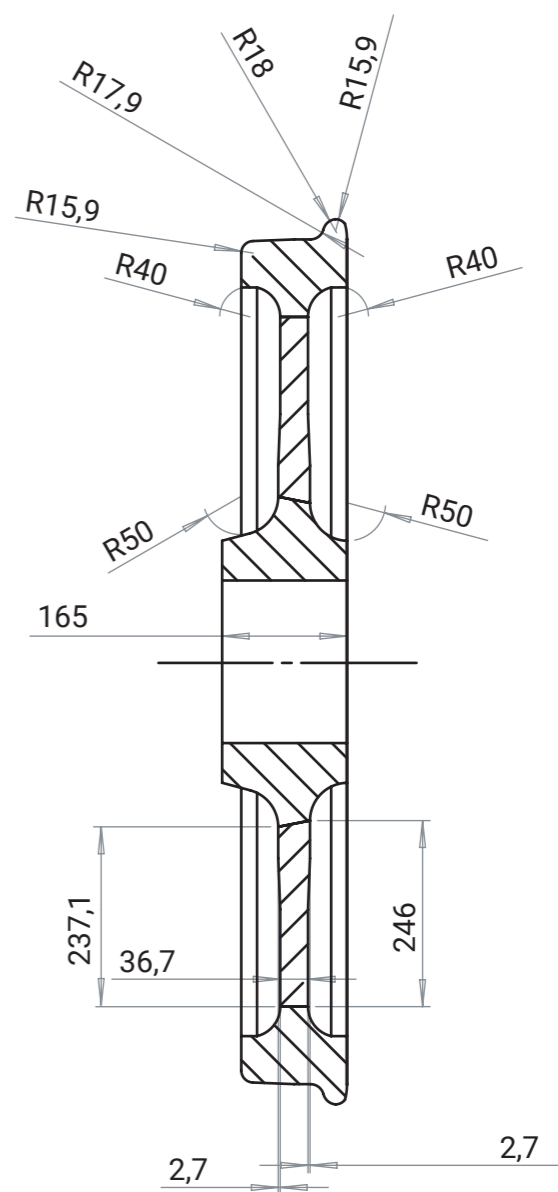
R17,9
R18
R15,9
R15,9
R40
R40
R50
R50
165
237,1
36,7
246
2,7
2,7
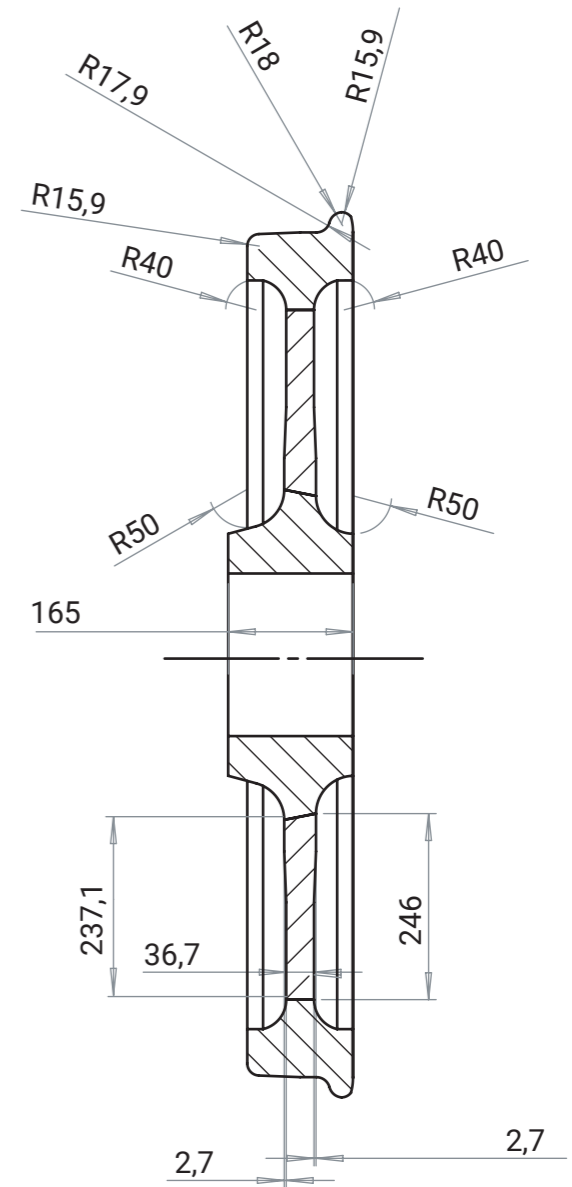
SECTION CUT A-A

SCALE   1 : 10

NOT SHOWN FILLETS: 0,5mm

ALL MEASUREMENTS IN mm

Nº UNITS	DESIGNATION		REFERENCE	MATERIAL		CODE
1	BASE WHEEL		III.1	UIC 812-3 R6 T,E		1
	DATE	SIGN	UNIVERSITAT POLITÈCNICA DE VALÈNCIA			
DRAWN	23/05/17					
CHECKED	23/05/17					
SCALE	UNPERFORATED WHEEL			TOLERANCE:	+0,5mm +1°	
				DRAWING Nº		
1:10				1		A3

Ø 1112,7
Ø 990
Ø 912
Ø 654,8
Ø 436,5
Ø 320
Ø 215
Ø 1170,5
25,1°
36°

14 EQUIDISTANT Ø 76 PERFORATIONS
10 EQUIDISTANT Ø 73 PERFORATIONS

139,7
108,2
108,2

R17,9
R18
R15,9
R15,9
R40
R40
R50
R50
165
237,1
36,7
246
2,7
2,7

SECTION CUT A-A
SCALE   1 : 10

NOT SHOWN FILLETS: 0,5mm
ALL MEASUREMENTS IN mm

248,75
367,50

SECTION   B-B
SCALE   1 : 10

Nº UNITS	DESIGNATION		REFERENCE	MATERIAL	CODE
1	OPTIMAL WHEEL		III.2	UIC 812-3 R6 T,E	2
	DATE	SIGN	UNIVERSITAT POLITÈCNICA DE VALÈNCIA		
DRAWN	27/05/17				
CHECKED	27/05/17				

SCALE	OPTIMAL WHEEL	TOLERANCE:	+0,5mm +1°
1:10		DRAWING Nº 2	A3